RM-653

GROUND IMPINGEMENT OF A FAN JET EXHAUST PLUME

May 1978

RESEARCH DEPARTMENT

GRUMMAN AEROSPACE CORPORATION
BETHPAGE, NEW YORK

UNCLASSIFIED

SECURITY CLASSIFICATION OF THIS PAGE *(When Data Entered)*

REPORT DOCUMENTATION PAGE		READ INSTRUCTIONS BEFORE COMPLETING FORM
1. REPORT NUMBER RM-653	2. GOVT ACCESSION NO.	3. RECIPIENT'S CATALOG NUMBER
4. TITLE *(and Subtitle)* GROUND JET IMPINGEMENT OF A FAN JET EXHAUST PLUME		5. TYPE OF REPORT & PERIOD COVERED
		6. PERFORMING ORG. REPORT NUMBER RM-653
7. AUTHOR(s) William G. Hill, Jr. Richard C. Jenkins		8. CONTRACT OR GRANT NUMBER(s)
9. PERFORMING ORGANIZATION NAME AND ADDRESS Grumman Aerospace Corporation Research Department Bethpage, New York 11714		10. PROGRAM ELEMENT, PROJECT, TASK AREA & WORK UNIT NUMBERS
11. CONTROLLING OFFICE NAME AND ADDRESS		12. REPORT DATE May 1978
		13. NUMBER OF PAGES 49
14. MONITORING AGENCY NAME & ADDRESS*(if different from Controlling Office)*		15. SECURITY CLASS. *(of this report)* Unclassified
		15a. DECLASSIFICATION/DOWNGRADING SCHEDULE

16. DISTRIBUTION STATEMENT *(of this Report)*

Approved for Public Release; Distribution Unlimited

17. DISTRIBUTION STATEMENT *(of the abstract entered in Block 20, if different from Report)*

18. SUPPLEMENTARY NOTES

19. KEY WORDS *(Continue on reverse side if necessary and identify by block number)*

Jet Impingement; V/STOL

20. ABSTRACT *(Continue on reverse side if necessary and identify by block number)*

This report describes an investigation of the ground impingement properties of a fan jet engine exhaust. Measurements were taken using both a simulated fan jet of laboratory scale and a large scale operating fan jet engine. The results of this work will be used to modify existing models of exhaust-ground interactions to include the unique properties of fan jet impingement on the flow field under a hovering VTOL aircraft, with particular application to the Grumman Design 698. The simulated fan jet exhaust was produced by cold air issuing from a concentric nozzle

DD FORM 1 JAN 73 1473 EDITION OF 1 NOV 65 IS OBSOLETE
S/N 0102-014-6601 |

UNCLASSIFIED

SECURITY CLASSIFICATION OF THIS PAGE *(When Data Entered)*

and utilizing a screen in the inner section to develop the lower dynamic pressure that is characteristic of a real fan jet engine. Measurements taken during impingement of the jet engine exhaust consisted of pitot pressure profiles above the ground. Wall jet velocity profiles obtained in these two impingement flows showed close agreement when scaled by size and nozzle pressure ratio. This favorable comparison demonstrates the effectiveness of using cold air, scale model flows to simulate the impingement flow of an immersed control vane were investigated in both the simulated and the fan jet engine exhausts.

(14) Grumman Research Department Memorandum RM-653

(6) GROUND IMPINGEMENT OF A FAN JET EXHAUST PLUME.

by [illegible] Rept.,

(10) William G./Hill, Jr.

and

Richard C./Jenkins

Fluid Dynamics

(11) May [redacted]78

(12) 53p.

Approved by: Richard A. Scheuing
Richard A. Scheuing
Director of Research

406165

ABSTRACT

This report describes an investigation of the ground impingement properties of a fan jet engine exhaust. Measurements were taken using both a simulated fan jet of laboratory scale and a large scale operating fan jet engine. The results of this work will be used to modify existing models of exhaust-ground interactions to include the unique properties of fan jet impingement on the flow field under a hovering VTOL aircraft, with particular application to the Grumman Design 698. The simulated fan jet exhaust was produced by cold air issuing from a concentric nozzle and utilizing a screen in the inner section to develop the lower dynamic pressure that is characteristic of a real fan jet engine. Measurements taken during impingement of the jet engine exhaust consisted of pitot pressure profiles above the ground.

Wall jet velocity profiles obtained in these two impingement flows showed close agreement when scaled by size and nozzle pressure ratio. This favorable comparison demonstrates the effectiveness of using cold air, scale model flows to simulate the impingement flow field of a real fan jet engine exhaust. The effects on the impingement flow of an immersed control vane were investigated in both the simulated and the fan jet engine exhausts.

ABSTRACT

TABLE OF CONTENTS

Section		Page
1	Introduction	1
2	Laboratory Simulation of Fan Jet Exhaust Impingement	3
	Free Stream Measurements	5
	Impingement Properties Without Vane	5
	Impingement Properties With Vane	14
3	Wall Jet Properties Produced by Impingement of a Fan Engine Exhaust	25
4	Conclusions	35
5	References	37
Appendix	Characteristics of Wall Jets Formed by Circular Jet Impingement	A-1

LIST OF ILLUSTRATIONS

Figure		Page
1	Photo of Concentric Nozzle and Control Vane	3
2	Schematic of Concentric Nozzle and Control Vane	4
3	Concentric Nozzle Exhaust Profiles	6
4	Ground Pressure Distribution for Impingement Without Vane	7
5	Oil Flow Pattern Formed by Concentric Jet Impingement Without Vane	8
6	Comparison of Wall Jet Velocity Profiles	10
7	Wall Jet Azimuthal Variation for Concentric Jet Impingement.	12
8	Radial Wall Jet Behavior for Fan Jet Impingement	13
9	Sketch of Vane and Ground Coordinate System	15
10	Oil Flow Patterns	16
11	Ground Isopressure Contours for Impingement with Vane	18
12	Wall Jet Velocity Profiles, Concentric Nozzle	19
13	Wall Jet Profiles for Vane $\alpha_v = 0$	20
14	Wall Jet Profiles for Vane $\alpha_v = +20°$	21
15	Effects of Vane Deflection on Wall Jet Properties	22
16	Wall Jet Strength at h' =0.7 in	23
17	Ground Plane Used for Fan Jet Engine Impingement	26
18	Comparison of Wall Jet Data from Engine Tests with Profile Obtained from Laboratory Simulation	28
19	Radial Wall Jet Variation	29
20	Effect of Vane Angle on Maximum Wall Jet Velocities	30
21	Wall Jet Profiles	31
22	Effects of Vane Deflection on Wall Jet Properties	32
A-1	Sketch of Free Jet Ground Impingement	A-2

Figure		Page
A-2	Wall Jet Velocity Profiles	A-3
A-3	Effect of Ground Spacing on Wall Jet Characteristics	A-5
A-4	Effect of Jet Velocity on Radial Decay of Maximum Wall Jet Velocity	A-6
A-5	Effect of Jet Velocity on Wall Jet Growth	A-7

ACKNOWLEDGMENTS

The authors would like to thank Ray Rice, Program Manager for the Q-fan engine impingement testing, for making possible our measurements during that program. We would also like to thank Charlie Schell, Harold Bell, John Gilbert, and Terry Jeanette for their help in setting up and conducting our "piggyback" tests.

Finally, we wish to thank our technician, George Homfeld, for his usual excellent assistance in fabricating and setting up both the scale model tests and our portion of the engine tests.

LIST OF SYMBOLS

d_f	exit diameter of fan or outer nozzle
d_N	exit diameter of round nozzle
h	spacing between ground and fan or outer nozzle exit
h'	normal distance above ground plane
$h'_{.5}$	value of h' for which $u/u_m = .5$ in wall jet profile
m	spacing between vane trailing edge and ground
n	exponent used in modeling radial variation of wall jet properties
p	local surface pressure on ground
p_A	ambient pressure
p_S	local static pressure
q	local dynamic pressure
q_c	dynamic pressure of inner nozzle flow
q_f	dynamic pressure of outer nozzle flow
q_j	exit dynamic pressure of a round jet
q_m	maximum dynamic pressure in a local wall jet profile
r	radial distance along ground from impingement centerline
r_p	probe radial location along ground from impact centerline
u	local velocity
u_f	velocity in outer nozzle flow at exit plane
u_m	maximum velocity in a local wall jet profile
x	distance normal to nozzle centerline, positive for $\phi = 180°$
y	distance normal to nozzle centerline, positive for $\phi = 90°$
z	distance along centerline from outer nozzle exit
α_v	vane angle of attack
ϕ	angular displacement, counterclockwise on ground plane, from negative x-axis

1. INTRODUCTION

Entrainment of ambient air into the engine exhausts of a VTOL aircraft hovering far from the ground develops negative pressures on the aircraft underside, exerting a downward force that opposes engine thrust. When the aircraft approaches the ground, several complicated effects arise. The exhaust jet plumes strike the ground and turn outward as wall jets. The entrainment of air into these wall jets, as well as the blockage of entrained air by the presence of the ground, leads to much larger downward (or suckdown) forces. This effect is not too difficult to understand and model. A much more complicated flow occurs when the wall jets from separate nozzles collide and send upwash and fountain flows back up toward the aircraft. These upward flows can deliver an upward force to the vehicle which reduces the suckdown force, or can even produce a net upward interference force. In addition, the heated exhaust gases that flow back toward the vehicle as part of these upwashes or fountains often reach areas where they can be entrained into the inlet flow and cause severe engine problems.

Flow properties in the upwash are controlled by conditions in the colliding wall jets, which are in turn controlled by jet exhaust impingement conditions. In Ref. 1 we described several methods of modeling the upwash in terms of wall jet properties and used existing empirical models (e.g., Refs. 2 and 3) to describe wall jet properties in terms of jet impingement conditions. This approach allows the upwash flow field (and eventually vehicle performance characteristics in ground effect) to be predicted directly from jet impingment conditions (Ref. 4).

The accuracy of such predictions is dependent on the model used to describe wall jet flow properties in terms of impingement conditions produced by a single incident jet. Existing models are based on data taken in a wall jet produced by impingement of a small scale, low temperature jet with uniform free stream conditions. The primary objective of this investigation was to determine the properties of a wall jet formed by impingement of a fan jet engine exhaust which exhibits a higher dynamic pressure in the fan flow than in the core flow. This type of propulsion system has been proposed for a Grumman Type "A" V/STOL aircraft configuration.

As a further complication to the impinging flow for this aircraft design, vehicle attitude control in hover is obtained by deflecting vanes that are immersed in the fan jet engine exhausts. Deflection of the exhausts by control vane inclination will distort the wall jet and upwash flow fields and alter the upwash force distribution on the aircraft. The present investigation also provides a preliminary assessment of wall jet distortion caused by vane deflection.

A two-phase experimental program was conducted to investigate the impingement properties of a fan jet engine exhaust. The first section of this report describes laboratory measurements obtained from impingement of a simulated fan jet exhaust produced by a four-inch diameter concentric nozzle. The second section describes the impingement flow produced with a 56-inch diameter high bypass ratio fan jet engine exhaust. A control vane was immersed in the exhaust for both sets of experiments.

For the laboratory experiments we used a concentric nozzle, fed by a common air supply, that was geometrically scaled to the jet engine configuration. Screens were used in the inner nozzle to reduce its exit velocity to provide the same dynamic pressure ratio between inner and outer flows as in the fan jet engine. The data consist of photographs showing oil flow ground streamline patterns, surface pressure contours, and wall jet pitot pressure profiles. These measurements were made for normal jet impingement with the ground plane located two diameters from the outer nozzle exit. Ground pressure distributions and wall jet growth produced by impingement of the concentric nozzle flow with and without the control vane are compared to uniform circular jet impingement properties, which are described in the Appendix.

The experiments with the fan jet engine exhaust were run to evaluate scale effects on wall jet properties. Data from the jet engine impingement tests consist of wall jet pitot pressure profiles obtained at two different radial stations above a 20 foot square ground plane. Comparison between these data and corresponding measurements made in the laboratory impingement flow showed that the wall jet profile shape and thickness growth rate was essentially the same in both flows, and that the radial decay in maximum velocity scaled with the nozzle dimensions.

2. LABORATORY SIMULATION OF FAN JET EXHAUST IMPINGEMENT

The exhaust flow from a high bypass ratio fan jet engine was simulated using air flow through a concentric nozzle that was geometrically similar to the engine nozzle downstream of the fan exit plane. Details of the fan jet engine being simulated will be given in Section 3. Figure 1 shows the concentric nozzle with a control vane mounted in its exhaust. A sketch showing the dimensions of this nozzle and the vane is shown in Fig. 2. The outer section of this nozzle had an elliptical entrance contour with a four inch ID for five inches upstream of the exit. The inner nozzle (1-5/8 inch ID) was supported inside the outer nozzle by thin webs (spider-type support) that were aligned with the flow. The air supply for the concentric nozzle was a low turbulence level settling chamber with a 2 foot square cross-section that was driven by a 7 hp centrifugal fan. The inner nozzle contained two fine-mesh screens to lower the core flow velocity to produce a dynamic pressure ratio q_f/q_c greater than 1, where the subscript f refers to the outer (fan) flow and c refers to the central flow.

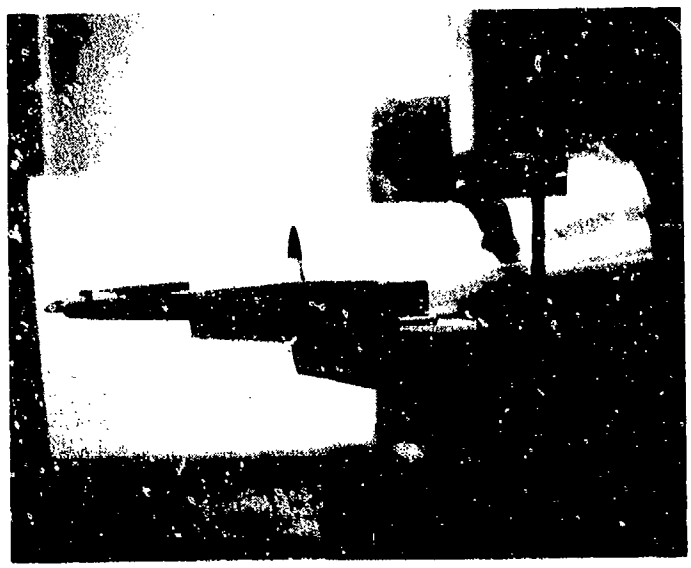

Figure 1 Photo of Concentric Nozzle and Control Vane

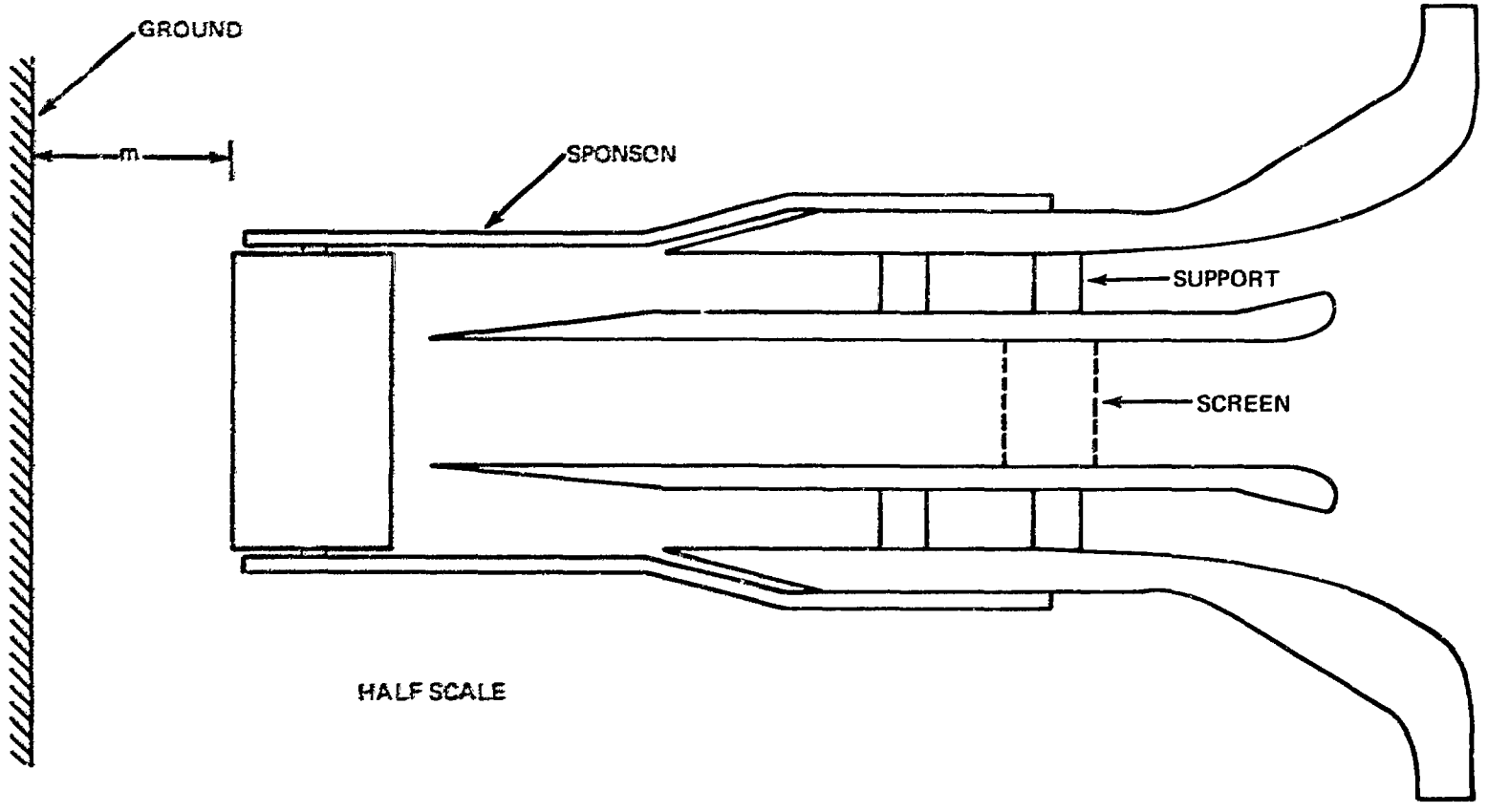

Figure 2 Schematic of Concentric Nozzle and Control Vane

FREE STREAM MEASUREMENTS

Measurements of free stream flow properties were taken in the exhaust of the concentric nozzle, without the vane, for a settling chamber pressure ratio of 1.045 (producing 283 ft/sec velocity at the exit of the outer nozzle). Figure 3a shows velocity profiles that were taken at two axial stations with a hot film anemometer. The data are normalized by the velocity at the exit of the outer nozzle, designated u_f. The screen blockage for the inner nozzle was chosen to produce a dynamic pressure ratio q_f/q_c of approximately 6 at $z/d_f = 2$, which was the ground location chosen for subsequent impingement work. Figure 3a shows a free stream velocity profile at this axial station. A second velocity profile shown for $z/d_f = .75$ shows that at the exit of the core nozzle the dynamic pressure ratio was close to 12. At the core exit the static pressure level was above ambient, as shown by the profile in Fig. 3b. Downstream of the core nozzle exit plane the static pressure decayed rapidly to ambient within a few inches as the core flow accelerated to a higher level.

IMPINGEMENT PROPERTIES WITHOUT VANE

Normal impingement of this type of flow produces a pressure distribution on the ground plane that differs from the usual axisymmetric, bell-shaped curve that is characteristic of conventional uniform jet impingement (see, e.g., Ref. 5). Figures 4a and 4b show ground pressure profiles found using a ground plane separation distance of $h/d_f = 2$. Figure 4c shows isopressure contours on the ground plane. The surface pressure distribution has a high pressure ring around most of the inner protion with lower pressures found near the centerline. The lower pressures in the center are caused by the low q region in the incident flow. This type of impingement pressure profile was also observed by Donaldson and Snedeker (Ref. 3) for supersonic round jets. In their case the low q region in the center was produced by pressure losses through a normal shock. Their investigation of the impingement flow revealed a breakdown in axial symmetry, with nodes forming in the high pressure ring through which the lower energy central flow escaped to the outer region.

(a) VELOCITY PROFILES

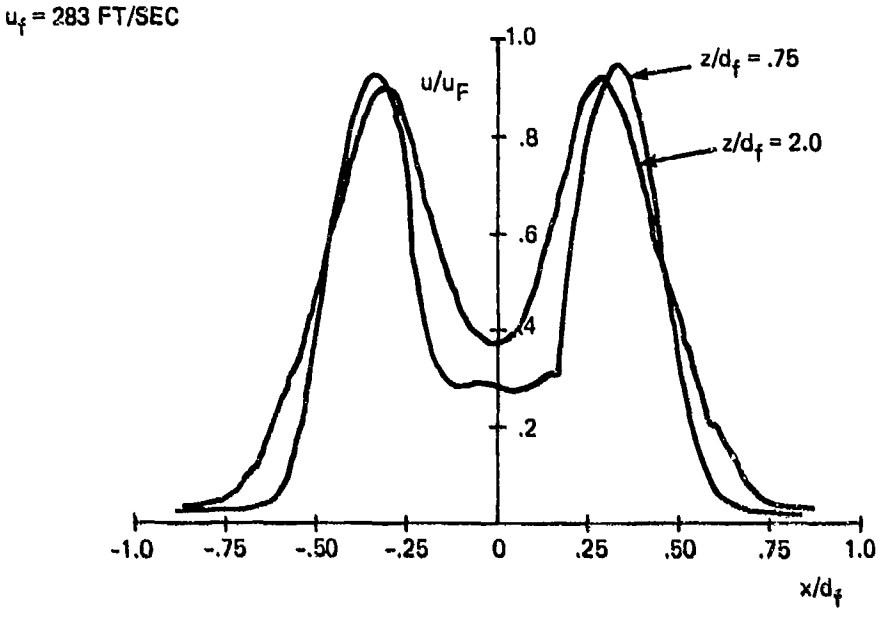

(b) STATIC PRESSURE PROFILE

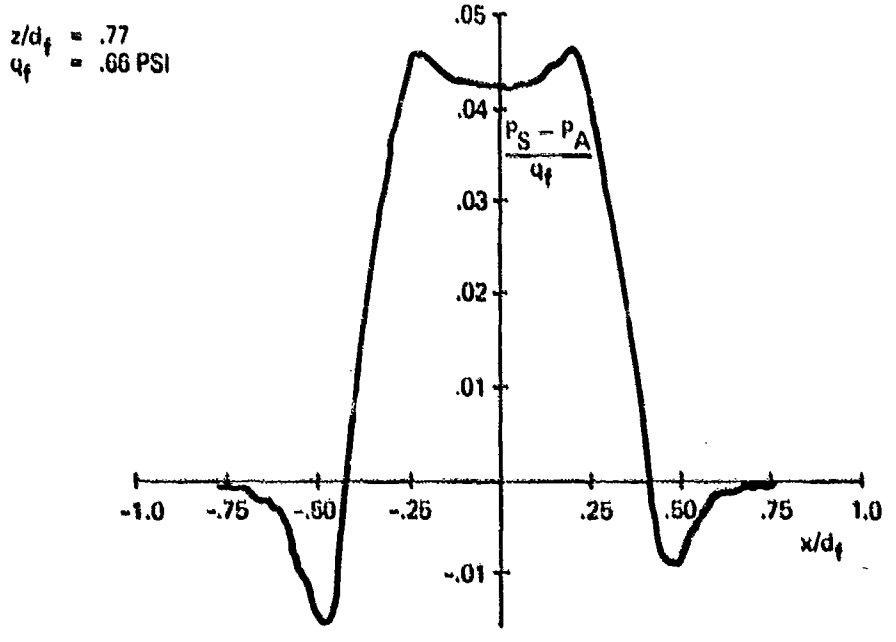

Figure 3 Concentric Nozzle Exhaust Profiles

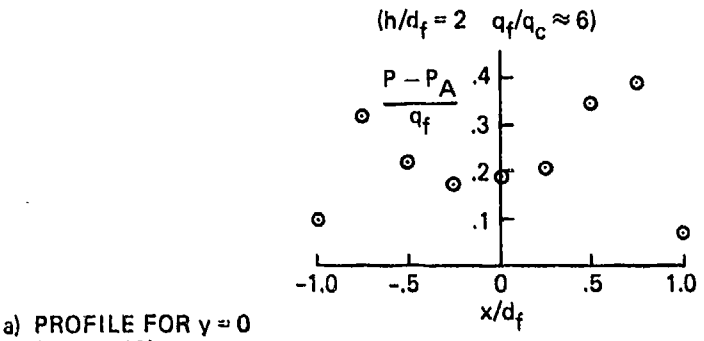

a) PROFILE FOR y = 0
(ϕ = 0, 180)

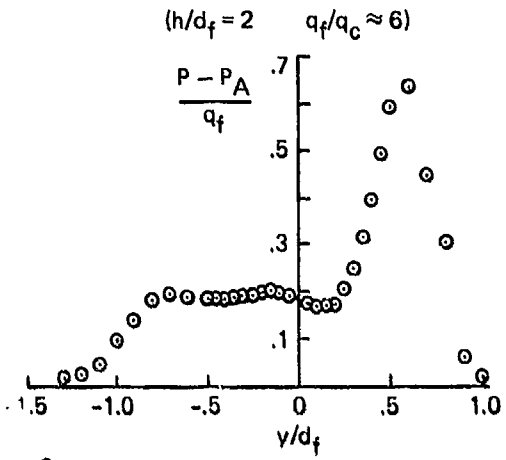

b) PROFILE FOR x = 0
(ϕ = ±90)

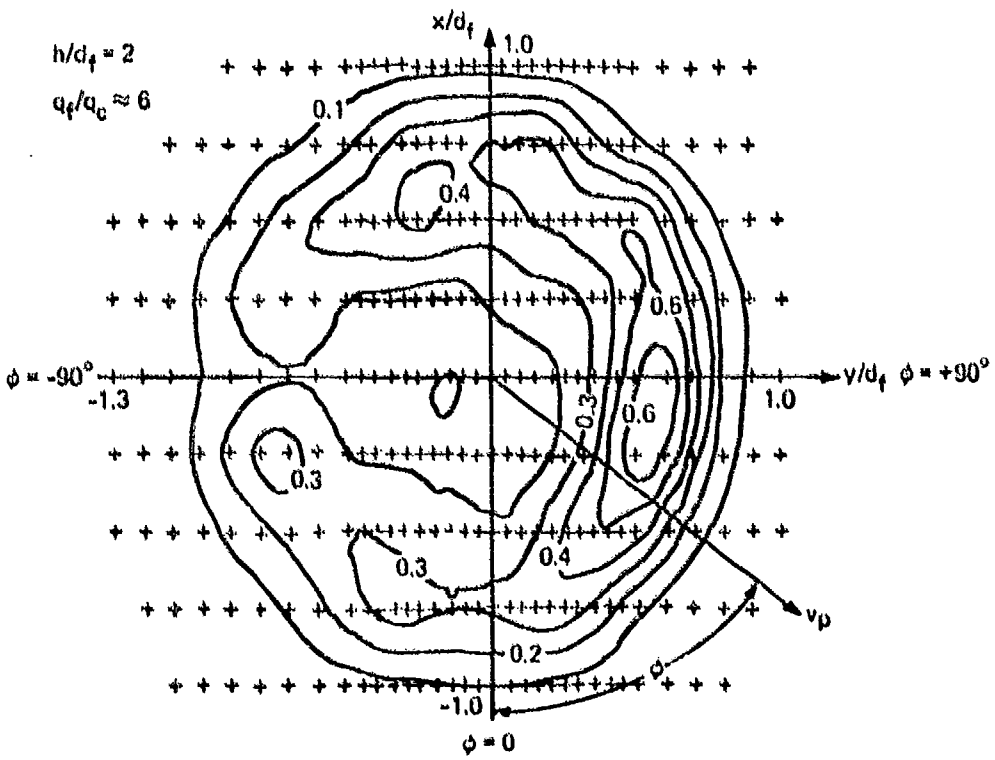

c) ISOPRESSURE CONTOURS

Figure 4 Ground Pressure Distribution for Impingement Without Vane

In our case the low q region in the center was produced by the screens in the inner nozzle. We also found that the flow arriving at the ground in the central region (lower dynamic pressure) had to bypass the high pressure ring to enter the wall jet region, but the way in which this was accomplished appeared somewhat different than described in Ref. 3. Strong deviations from axial symmetry are evident in Fig. 4 and in the corresponding oil flow pattern shown in Fig. 5. The heavy lines in this pattern formed almost immediately and were a repeatable part of the pattern providing the geometry (spider orientation, nozzle alignment, etc.) was left unchanged. The heavy concentration of oil splattered around $\phi = -90°$ (left side of photo) was sporadically accumulated during operation, and indicates the use of excessive oil.

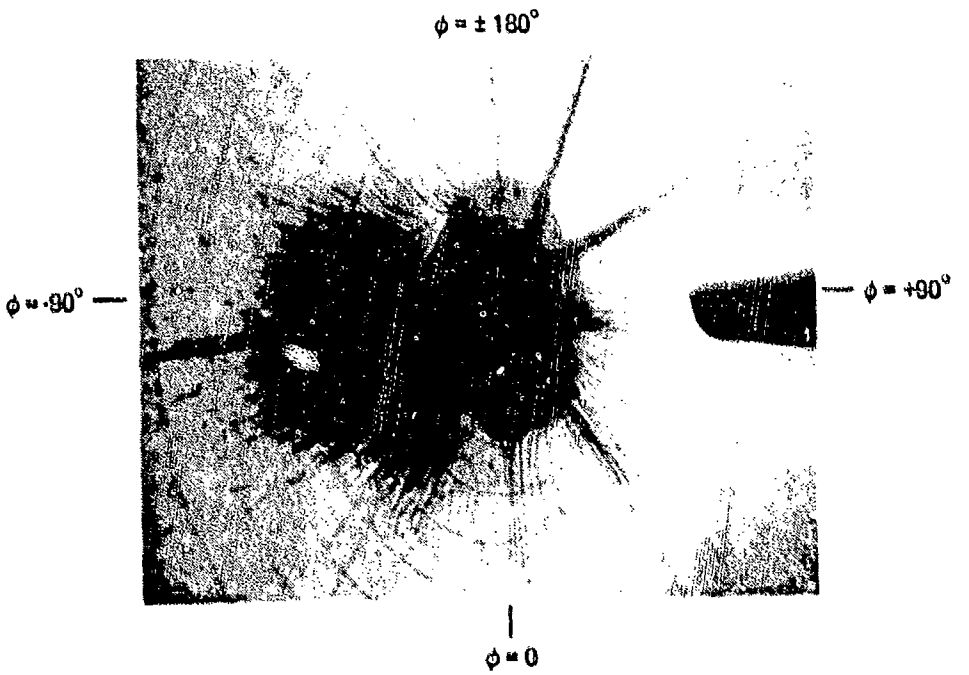

Figure 5 Oil Flow Pattern Formed by Concentric Jet Impingement Without Vane

The complex flow in the impact and transition regions does exhibit a node structure similar to that reported in Ref. 3. Wall jet pitot pressure profiles taken subsequently in the outer region with the same nozzle flow conditions and impingement orientation revealed a local thickening of the wall jet in regions where the heavy oil lines existed. Further probing with silk tufts showed that in the vicinity of the heavily concentrated oil lines the wall jet extended considerably above the ground, while in neighboring regions the flow at the same height above ground exhibited the strong fluctuations and velocity reversals that exist just beyond the edge of the wall jet.

Therefore the ground plane flow as not axially symmetric even though the impinging flow was symmetric and directed normal to the ground. The lack of symmetry appeard to occur because flow with lower dynamic pressure in the core of the incident flow escaped from the center of the impact region through locally thickened regions of the ground flow. The structure of local wall jet disturbances was very sensitive to small changes in ground plane location or orientation.

In order to evaluate wall jet distortions introduced by the presence of a vane in the fan jet exhaust flow (described in the next section) we adopted the following methods in our experimental procedure. First, all impingement tests with and without the vane were run without disturbing the ground plane or nozzle orientation. Second, the wall jet disturbances without the vane were documented so that additional disturbances introduced by the vane could be identified. The following paragraphs provide a detailed description of the wall jet characteristics observed without the vane for impact zone conditions described by Figs. 4 and 5. These characteristics are compared to those observed in a wall jet formed by round jet impingement (Appendix) using the latter flow as a standard for evaluation of the effects of lowered core velocity on wall jet properties.

Figure 6 shows a comparison between data taken with a pitot tube in the wall jet region at $\phi = -90°$, corresponding to the strongest discrete oil line location, and at $\phi = +90°$ where there was no apparent oil line. These are shown compared to a velocity profile in a wall jet formed by normal

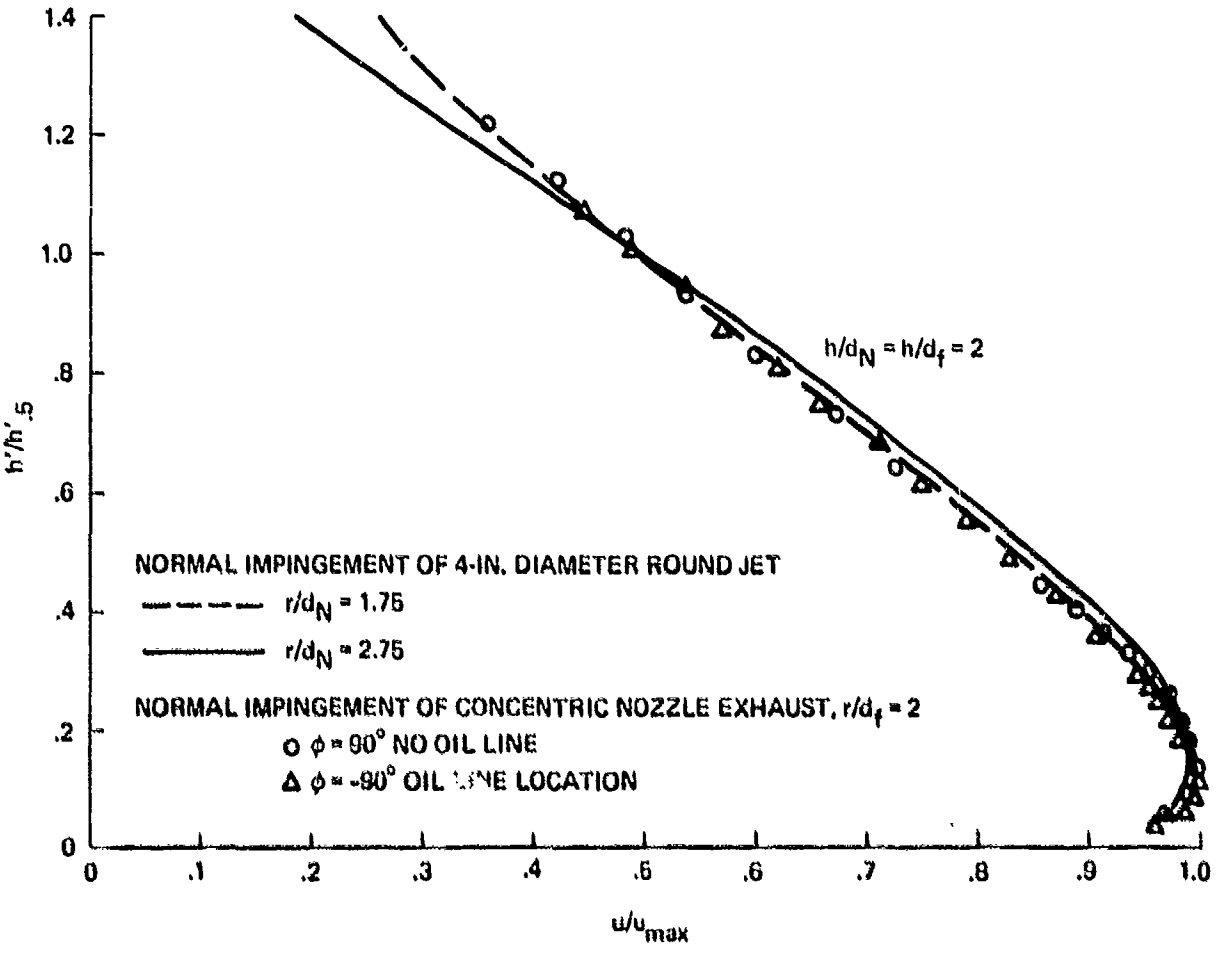

Figure 6 Comparison of Wall Jet Velocity Profiles

impingement of a round jet. The close agreement between profiles shows that a well-developed wall jet appears at the radial location $h/d_f = 2$ in spite of the lowered core dynamic pressure in the incident flow. Hence, the wall jet region for fan jet impingement begins at about the same radial location based on fan diameter as we found for round jet impingement. The agreement between nondimensionalized velocity profiles taken at any chosen location with those taken at locations exhibiting local thickening is significant because it allows a complete local wall jet description in terms of maximum velocity u_m and half velocity thickness $h'_{.5}$. In addition, similarity of profile shapes between locally thickened regions and undisturbed regions suggests that the flow in each small azimuthal sector is independent of its neighbors.

The wall jet behavior around the lower two quadrants of the ground plane ($-90° < \phi < +90°$) is illustrated by plots of half-velocity thickness and maximum velocity versus ϕ as shown in Figs. 7a and 7b. The data were taken at a probe radial location of $r_p/d_f = 2$, which was far enough to ensure the existence of similarity in velocity profiles. The thickness distribution exhibits well defined peaks in the half-velocity thickness at the locations of all of the heavy oil line concentrations shown in Fig. 5, the major peak existing at $\phi = -90°$. The maximum velocity profile shows local minimums at these points, but these minimums are not as well defined as the thickness spikes. The triangular symbol on the ordinate of each curve represents the maximum velocity and half-velocity thickness that were measured for a four-inch diameter round jet. To present this point in Fig. 7a we assumed that the round jet exit velocity was equal to u_f, hence the indicated value is high. The square symbol represents this ground plane measurement from round jet tests when the difference in exit plane momentum relative to the concentric nozzle has been accounted for.

The velocity decay and thickness growth of the wall jet at $\phi = -90°$ and at $\phi = +90°$ are compared in Figs. 8a and 8b (same impingement conditions as Figs. 4 to 7). For $\phi = -90°$, corresponding to the strongest oil line concentration, the maximum velocity is slightly lower and the thickness is considerably greater than at $\phi = +90°$. Figure 8b shows that in the

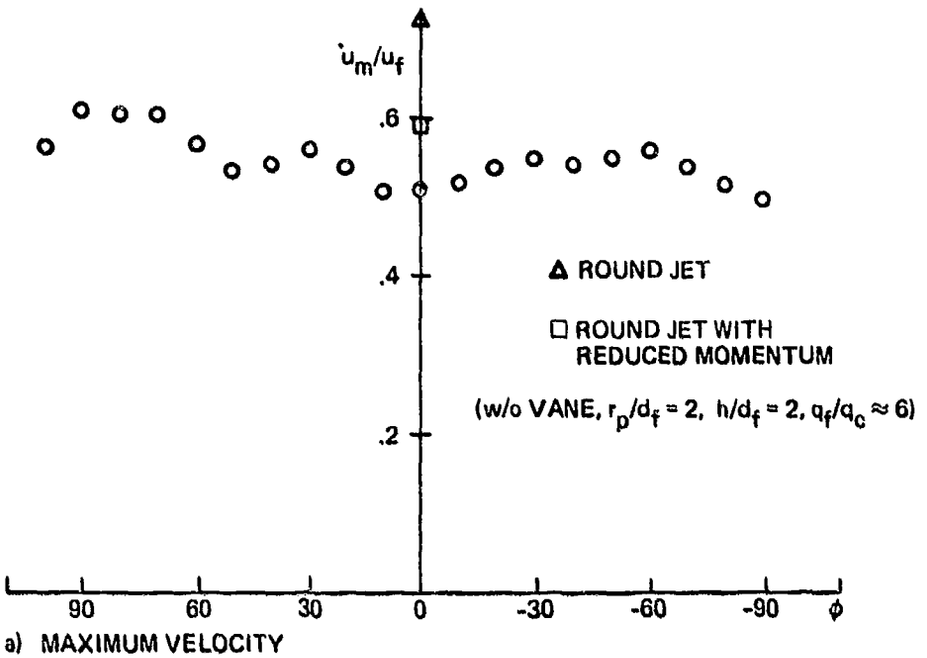

a) MAXIMUM VELOCITY

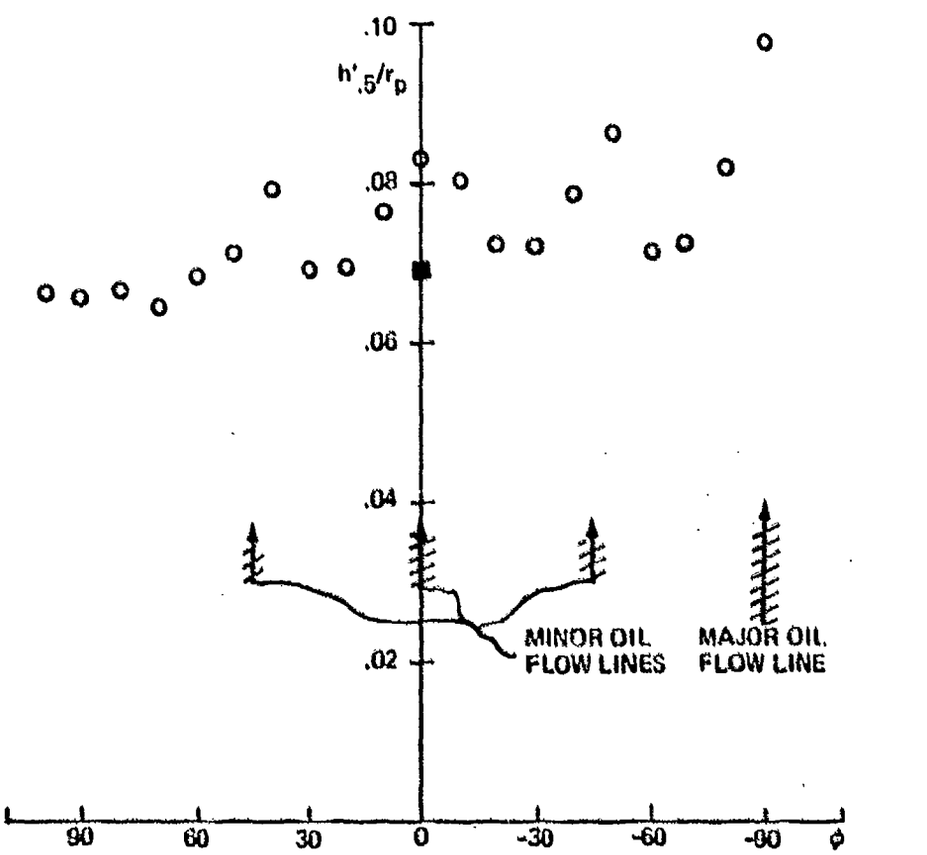

b) HALF VELOCITY THICKNESS

Figure 7 Wall Jet Azimuthal Variation for Concentric Jet Impingement

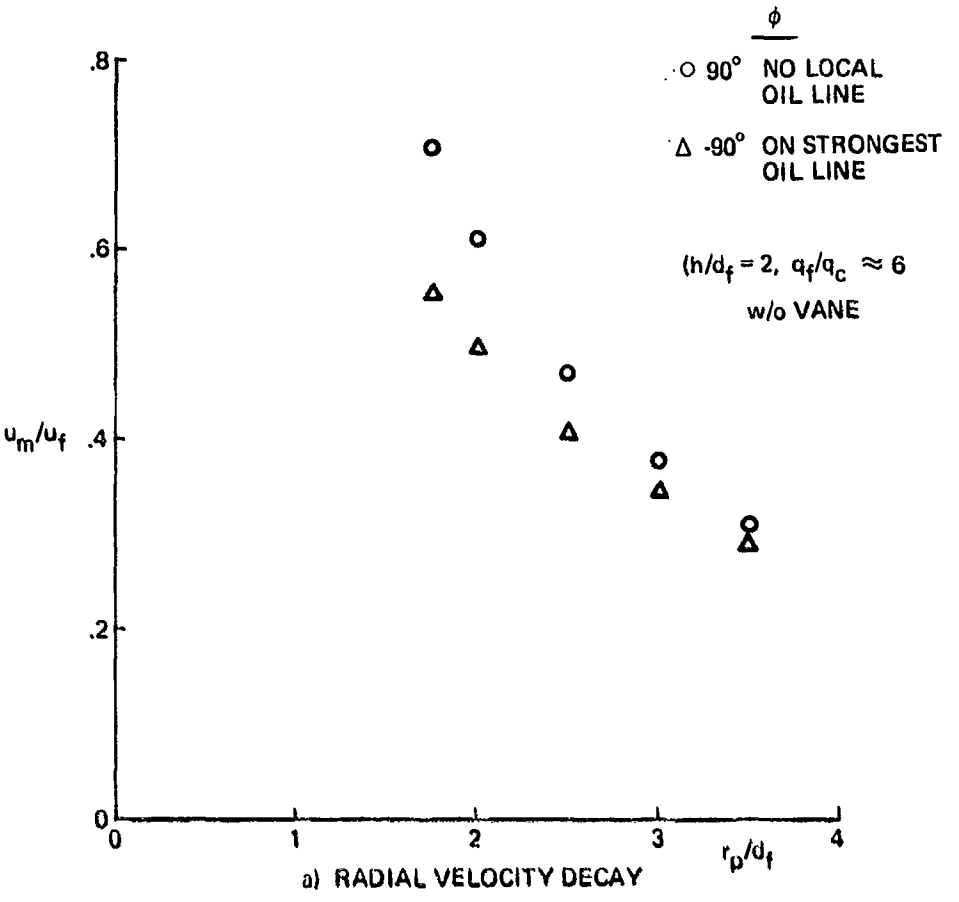

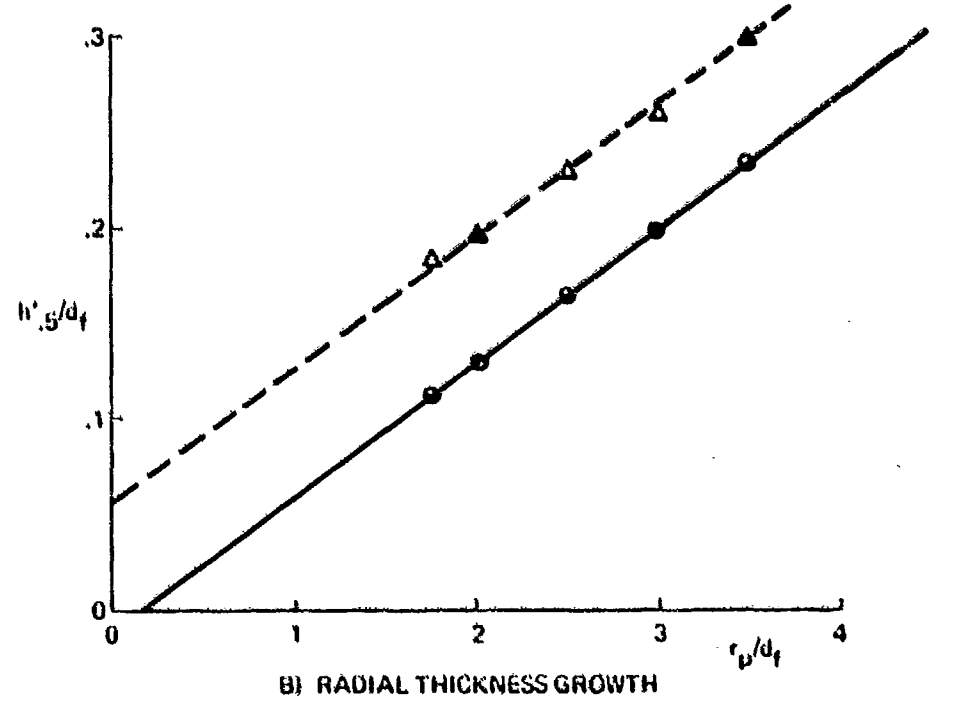

Figure 8 Radial Wall Jet Behavior for Fan Jet Impingement

vicinity of an oil line concentration the wall jet grows linearly but that it appears to originate from a point further away than the geometric center of the impact region. The radial decay in maximum velocity, when plotted in logarithmic coordinates, is linear with a lower slope near an oil line than away from an oil line. Assuming the radial maximum velocity variation $u_m \sim r^n$, we found $n = -.95$ at $\phi = -90°$ compared to $n = -1.2$ for $\phi = +90°$, the latter value providing good agreement with our data obtained with round jet impingement.

Hence, the flow in the wall jet region is radial but is not axially symmetric because of several local regions in which the flow along the ground is locally thicker, allowing flow with lower dynamic pressure to escape from the central region. We were unable to trace these locally thick regions to the wake of the spider supports. The heavy oil line pattern (slightly different when the spider support was realigned) appeared to be triggered by a slight axial misalignment of the inner and outer nozzles.

IMPINGEMENT PROPERTIES WITH VANE

A simulated control vane, 10 percent thick, with a two-inch chord and four-inch span, was supported at the outer edges by sponsons as shown in Fig. 2. The vane was attached to the sponsons by a rod passing through the half-chord point, which allowed the angle of attack α_v to be set before starting the flow. The vane was located on the nozzle centerline with its leading edge .28 inch from the exit of the central nozzle. The ground plane was located at distance m from the vane trailing edge, where m = 2.7 inches for the laboratory tests.

The vane used with the concentric nozzle was a simplified version of the actual control vane (described in the next section) used for the engine tests. We scaled the span, chord and thickness, but not the geared flap used for real engine tests. While this simplified vane did not allow us to simulate the full scale wall jet behavior at corresponding angles of attack, it did provide simulation for vane $\alpha_v = 0$ and it did allow us to investigate the general effects of an immersed vane on impingement properties.

Figure 9 shows a sketch of the ground coordinate system used to describe the impingement conditions. The line $\phi = 0$ (and $\phi = 180°$) was chosen parallel to the chord trailing edge. As indicated in the figure, positive vane angles of attack should be expected to deflect part of the flow toward negative values of y where ϕ is negative.

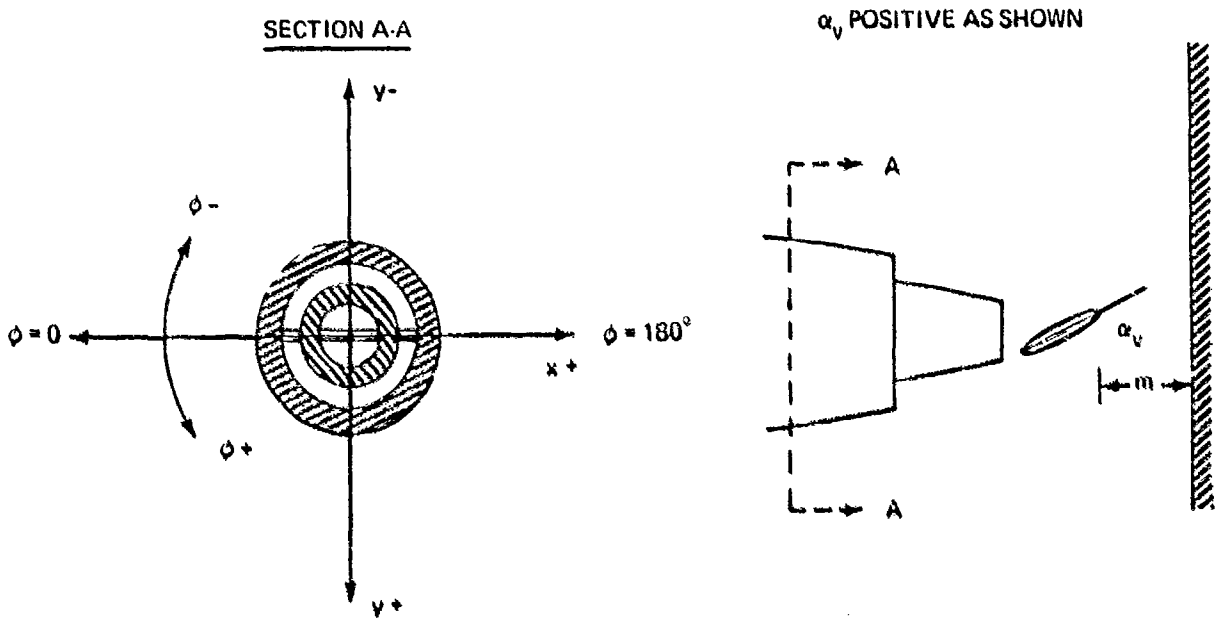

Figure 9 Sketch of Vane and Ground Coordinate System

Figure 10 shows the oil flow patterns produced with the vane at different angles of attack, using impingement conditions identical to those described in Impingement Properties Without Vane, except for the presence of the vane. In Fig. 10a, with $\alpha_v = 0$, the strong oil line close to $\phi = -90°$ is predominant, but the other lines observed in Fig. 5 (without the vane) have been suppressed. The patterns obtained with $\alpha_v = +20°$ and $-20°$ are shown in Figs. 10b and 10c. Note the emergence of lines close to $\phi = 0$ and $\phi = 180°$ in both cases, which are slightly inclined away from the direction of flow deflection.

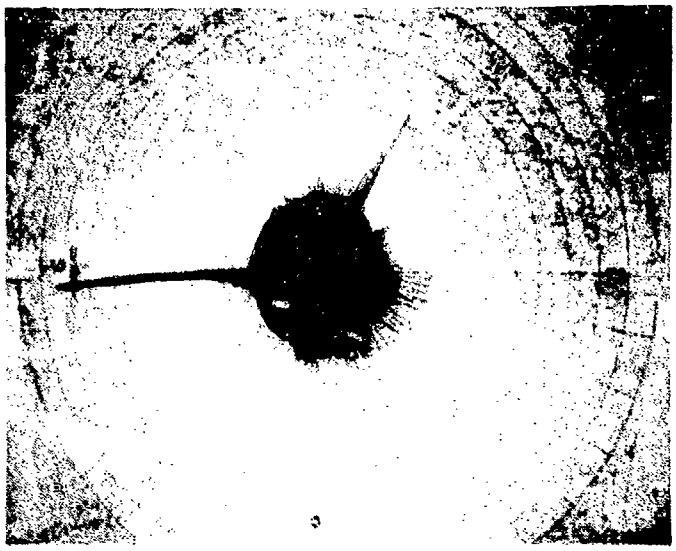

a) PATTERN FOR $\alpha_v = 0$

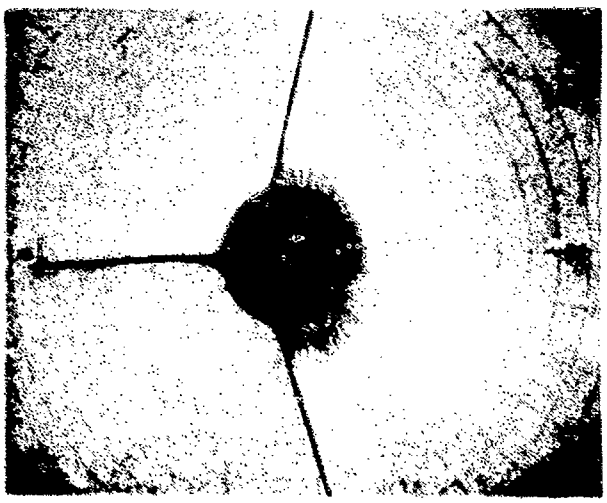

VANE DEFLECTS INCIDENT FLOW IN THIS DIRECTION

b) PATTERN FOR $\alpha_v = +20°$

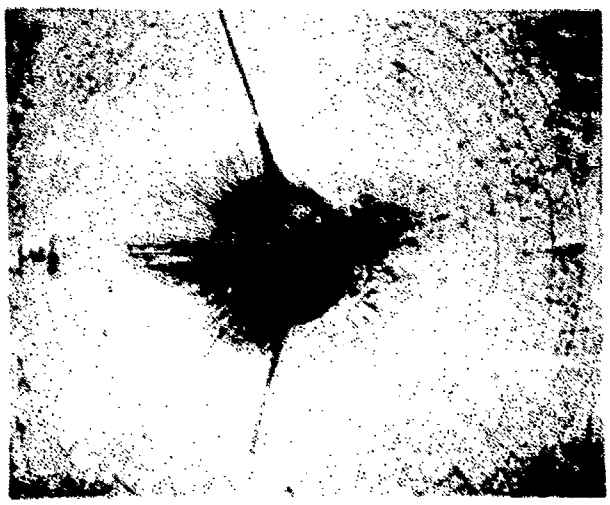

VANE DEFLECTS INCIDENT FLOW IN THIS DIRECTION

c) PATTERN FOR $\alpha_v = -20°$

Figure 10 Oil Flow Patterns

Surface isopressure contours for impingement conditions corresponding to Figs. 10a and 10b are shown in Figs. 11a and 11b for vane $\alpha_v = 0$ and +20°. Comparison of Fig. 11a with Fig. 4c shows that the presence of the vane at $\alpha_v = 0$ does not significantly alter the ground plane pressure contour. However, when the vane is deflected to $\alpha_v = +20°$ (Fig. 11b) several high pressure regions are produced on the ground and axial symmetry is completely eliminated.

Pitot pressure surveys were made above the ground in the wall jet region to determine the effects of vane deflection on the circumferential distribution of wall jet properties. Figure 12 shows the effects of van deflection on velocity profile shapes at different azimuthal positions for $r_p/d_f = 2$. Note that all of the profiles appear similar except for that taken at $\phi = 90°$. The shape of this thinner profile suggests (see Fig. A-2 in Appendix) that in this region the wall jet may require more radial distance to achieve velocity profile similarity.

Figures 13a and 13b show pitot pressure profiles taken (at $r_p/d_f = 2$) in 10° increments for $-30° < \phi < +30°$ with the vane at $\alpha_v = 0$. The profiles exhibit a dependence on ϕ but appear similar in shape. Figures 14a and 14b show the effects of vane deflection $\alpha_v = +20°$ on the profiles. For negative values of ϕ (vane deflects flow in this direction) the wall jet momentum is reduced by vane deflection in the region $-20° < \phi < 0$, but increased for more negative values of ϕ that are exposed to the deflected incident jet. For positive values of ϕ the maximum wall jet velocity is decreased everywhere except around $\phi = 10°$, and in this region the wall jet is extremely thick. These effects are more clearly evident in Fig. 15 in which we have plotted maximum dynamic pressure q_m and the half-velocity thickness $h'_{.5}$ as functions of ϕ. In these plots r_p represents the distance along the ground plane from the impact center to the probe location (8 inches). Figure 16 shows circumferential pitot pressure profiles that were taken at $h' = .7$ inches and $r_p/d_f = 2$, showing that the locally thickened wall jet region is located very close to $\phi = 10°$, where a very heavy oil line appears in Fig. 10b due to vane deflection.

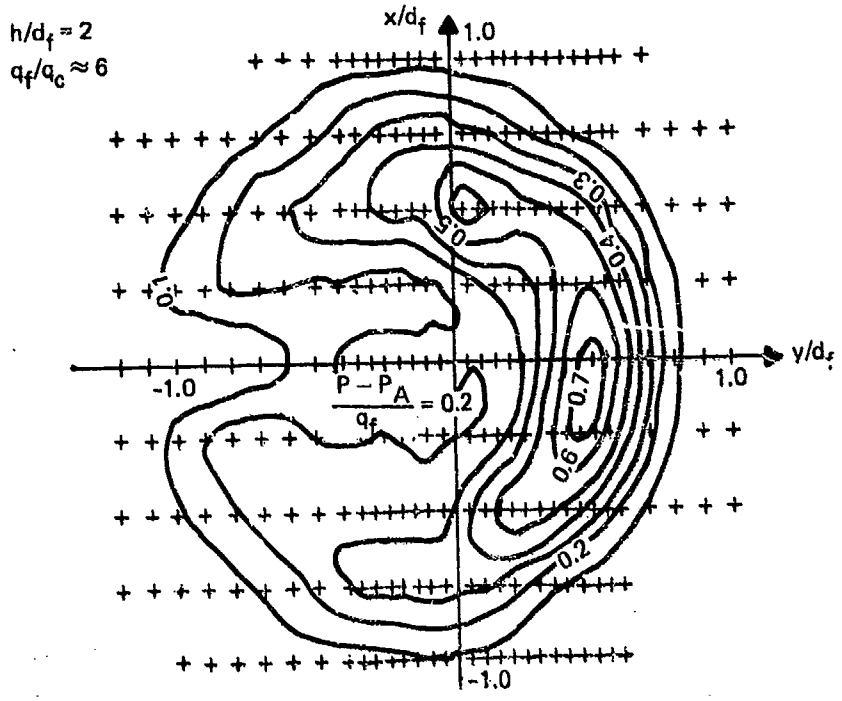

a) Vane Angle, $\alpha_v = 0°$

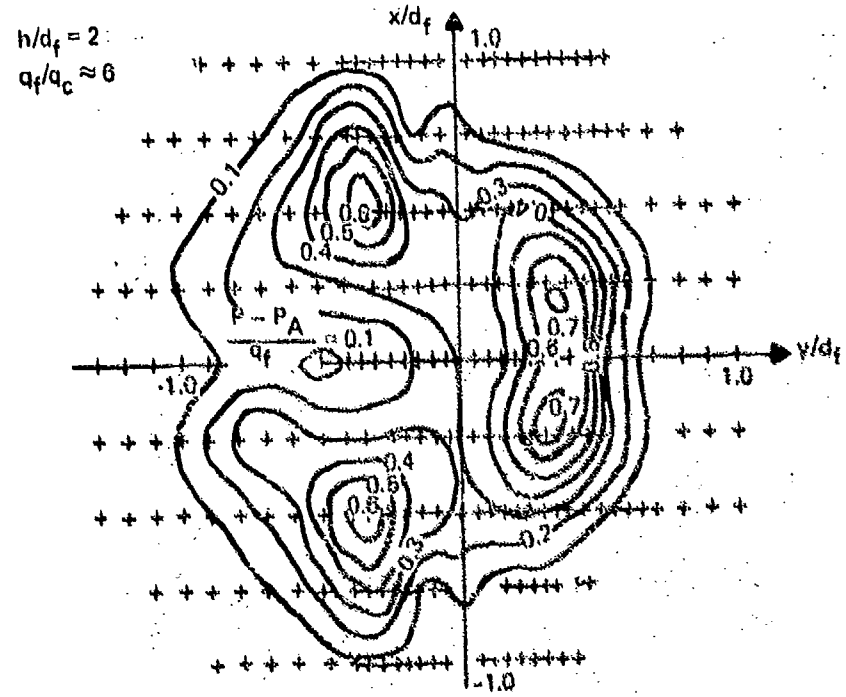

b) Vane Angle, $\alpha_v = 20°$

Figure 11 Ground Isopressure Contours for Impingement With Vane

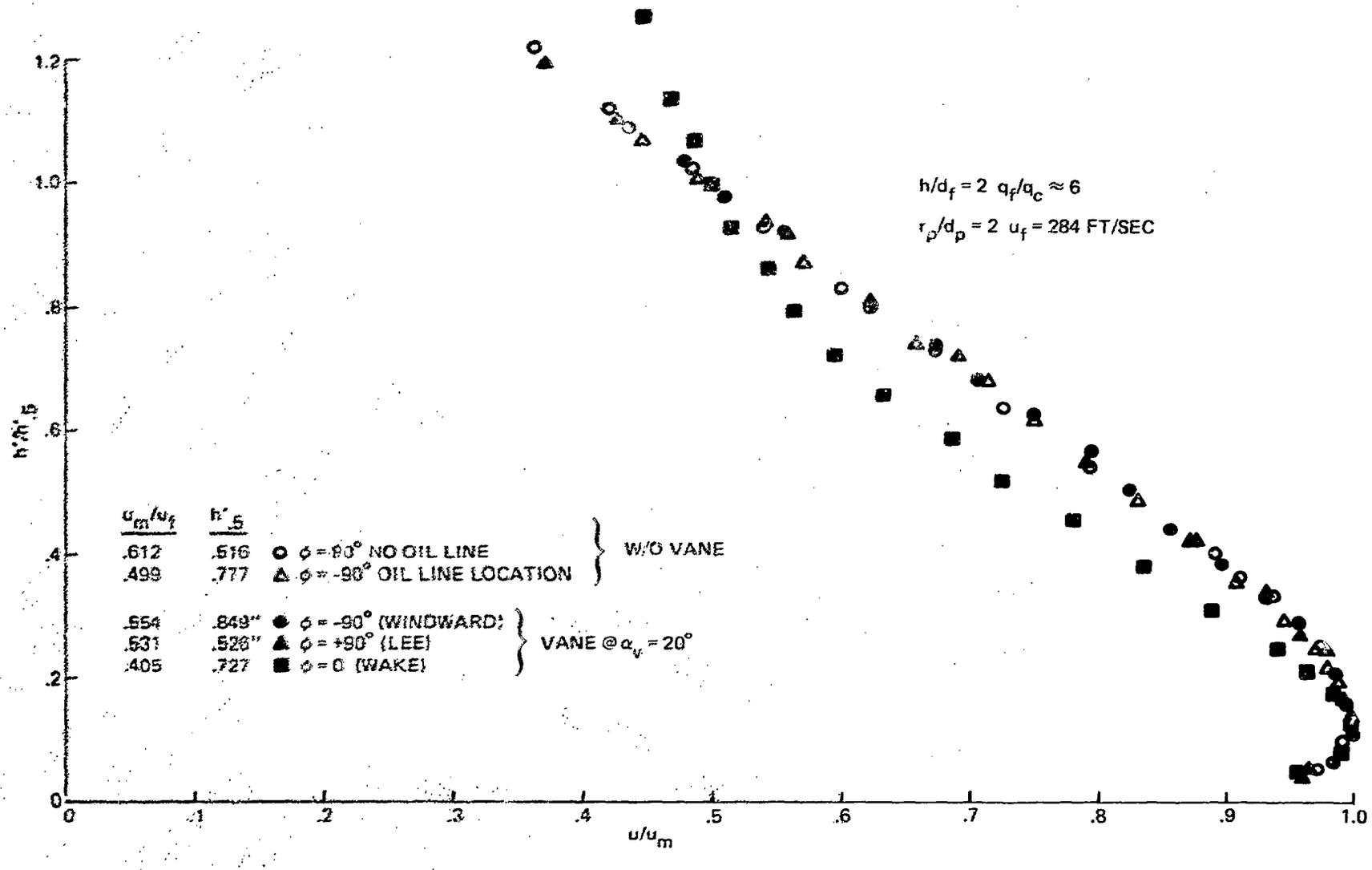

Figure 12 **Wall Jet Velocity Profiles, Concentric Nozzle**

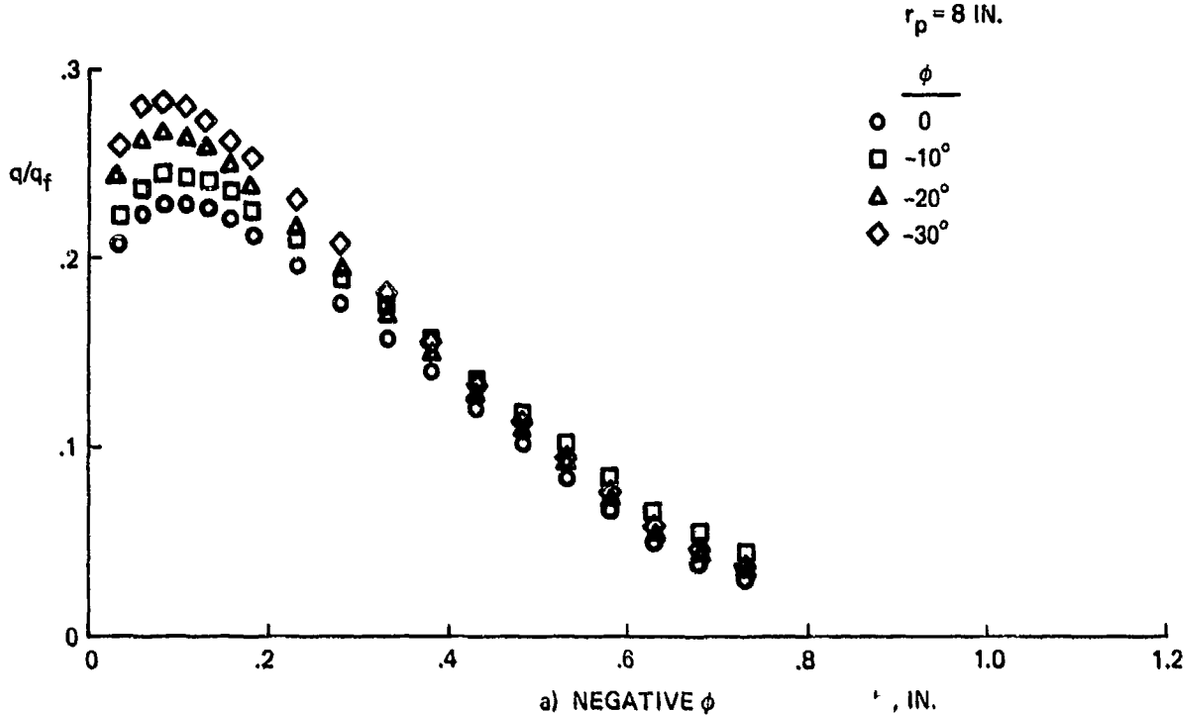

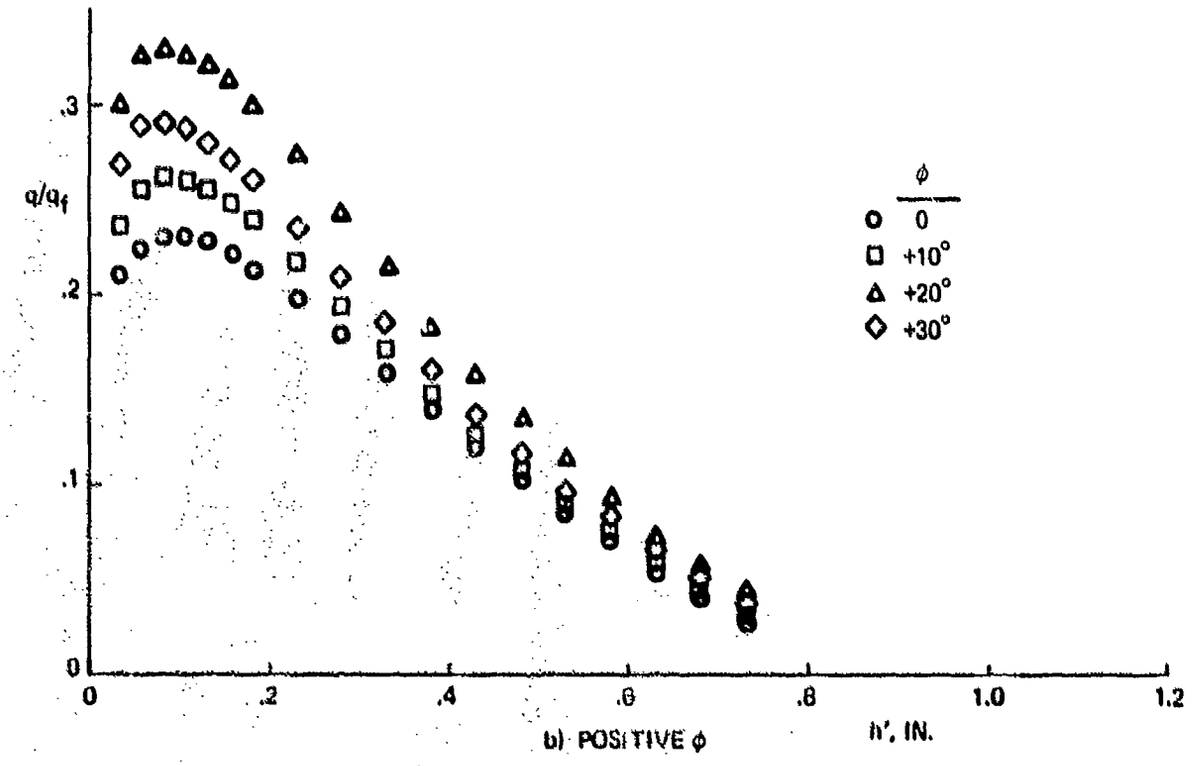

Figure 13 Wall Jet Profiles for Vane α_v = 0

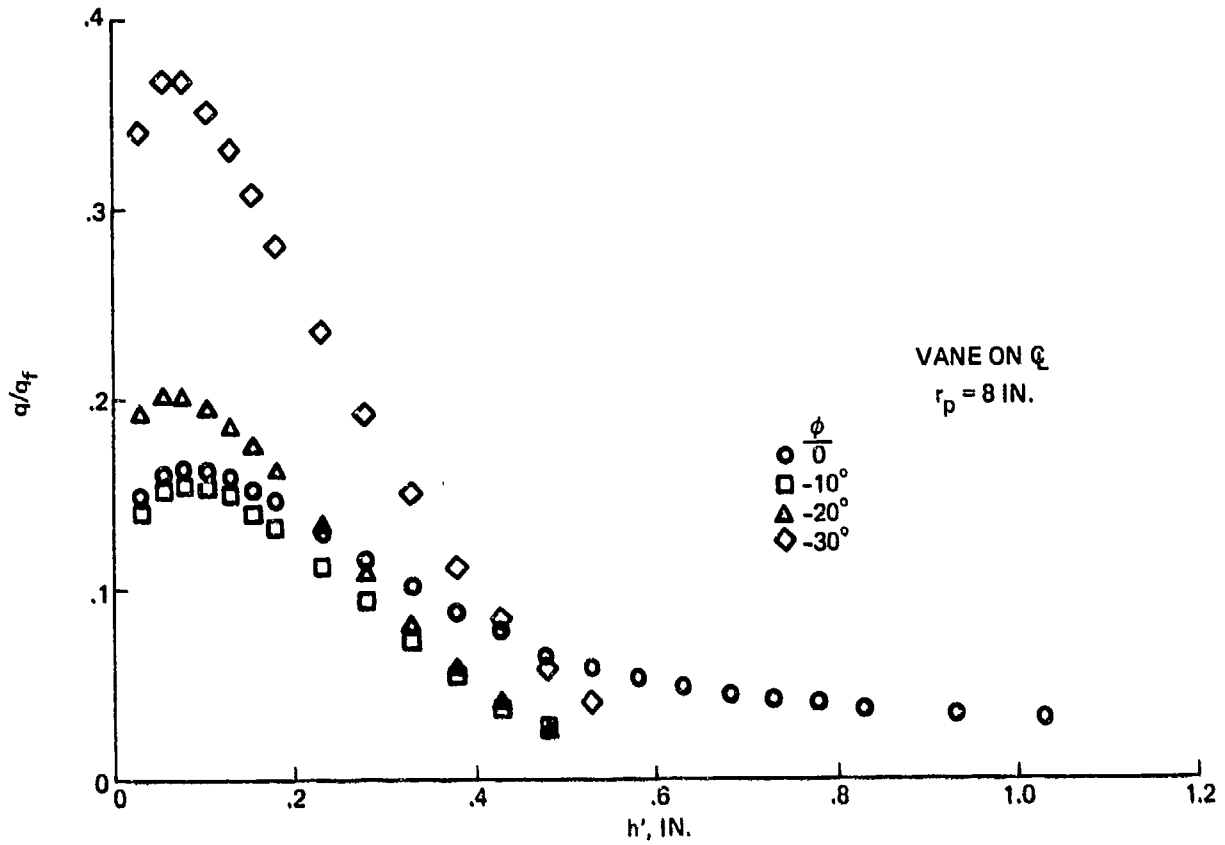

a) VANE DEFLECTS FLOW IN THIS DIRECTION

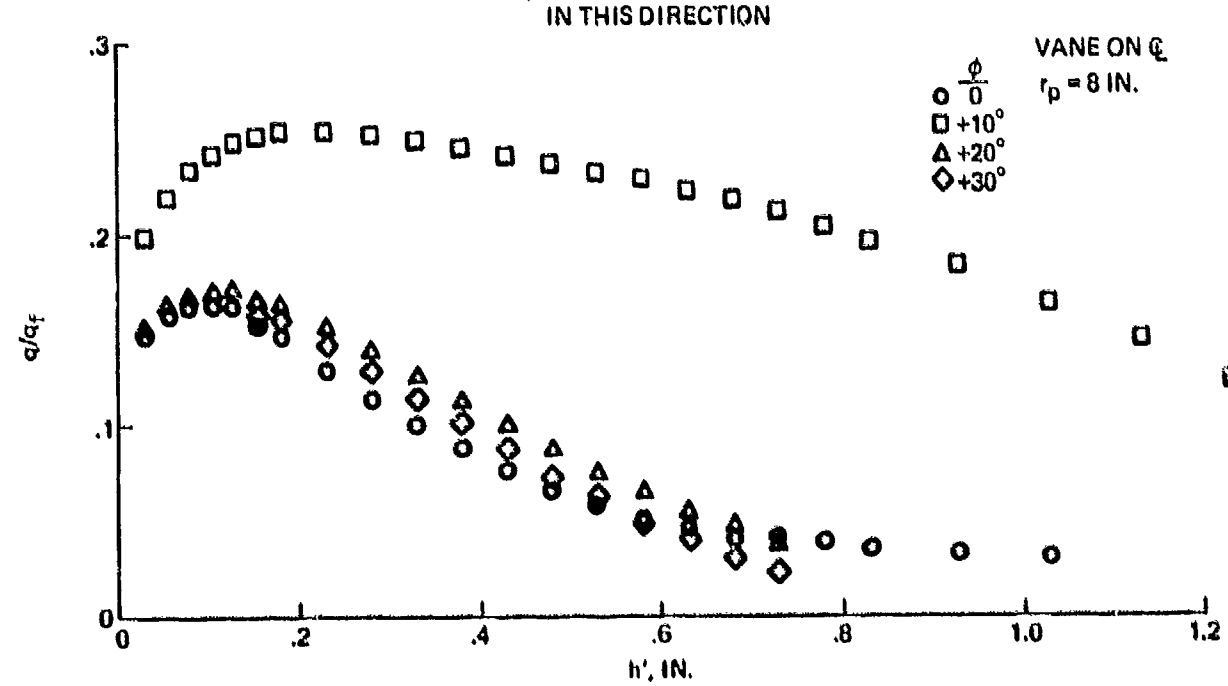

b) VANE DEFLECTS FLOW AWAY FROM THIS DIRECTION

Figure 14 Wall Jet Profiles for Vane α_v = +20°

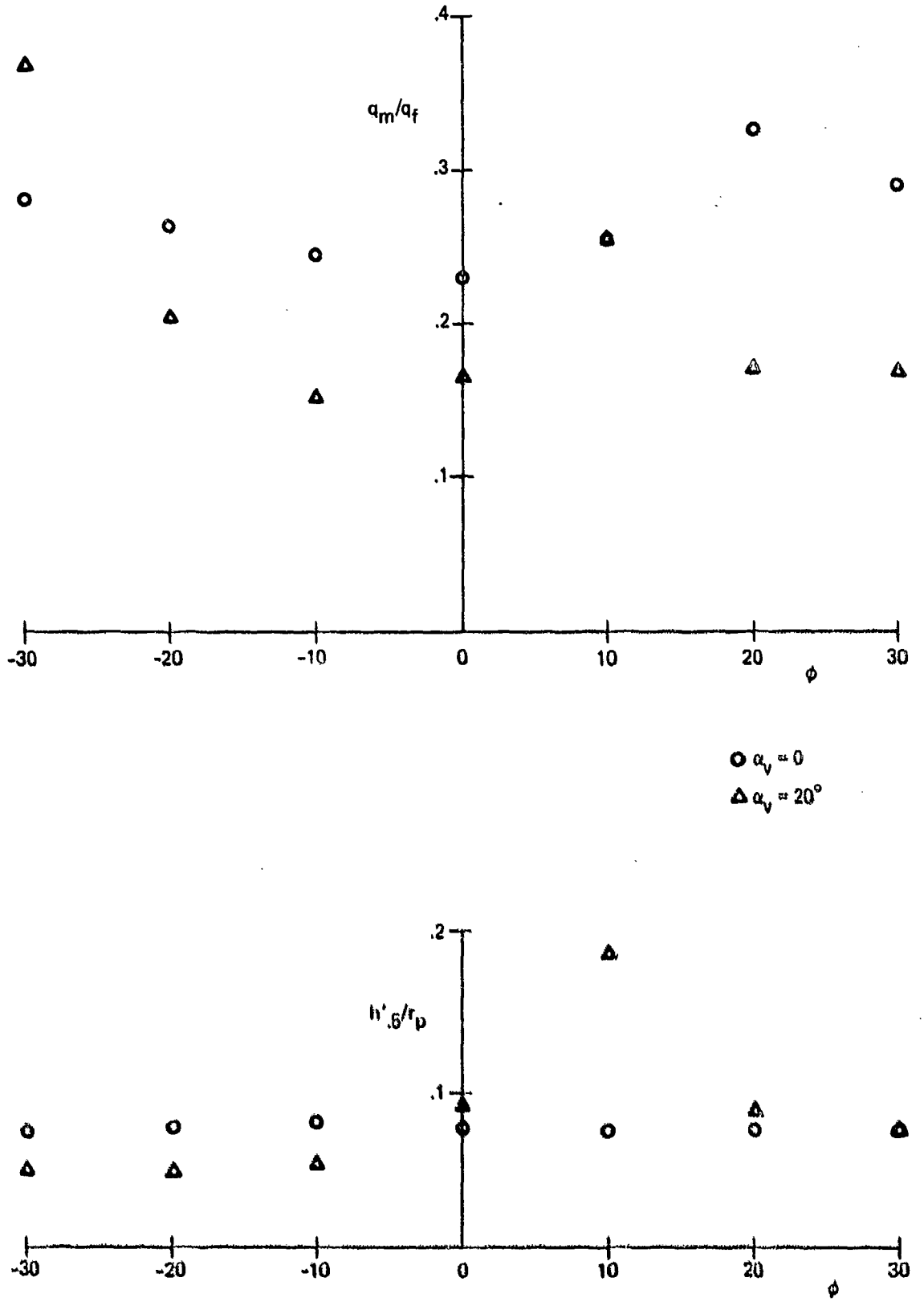

Figure 15 Effects of Vane Deflection on Wall Jet Properties

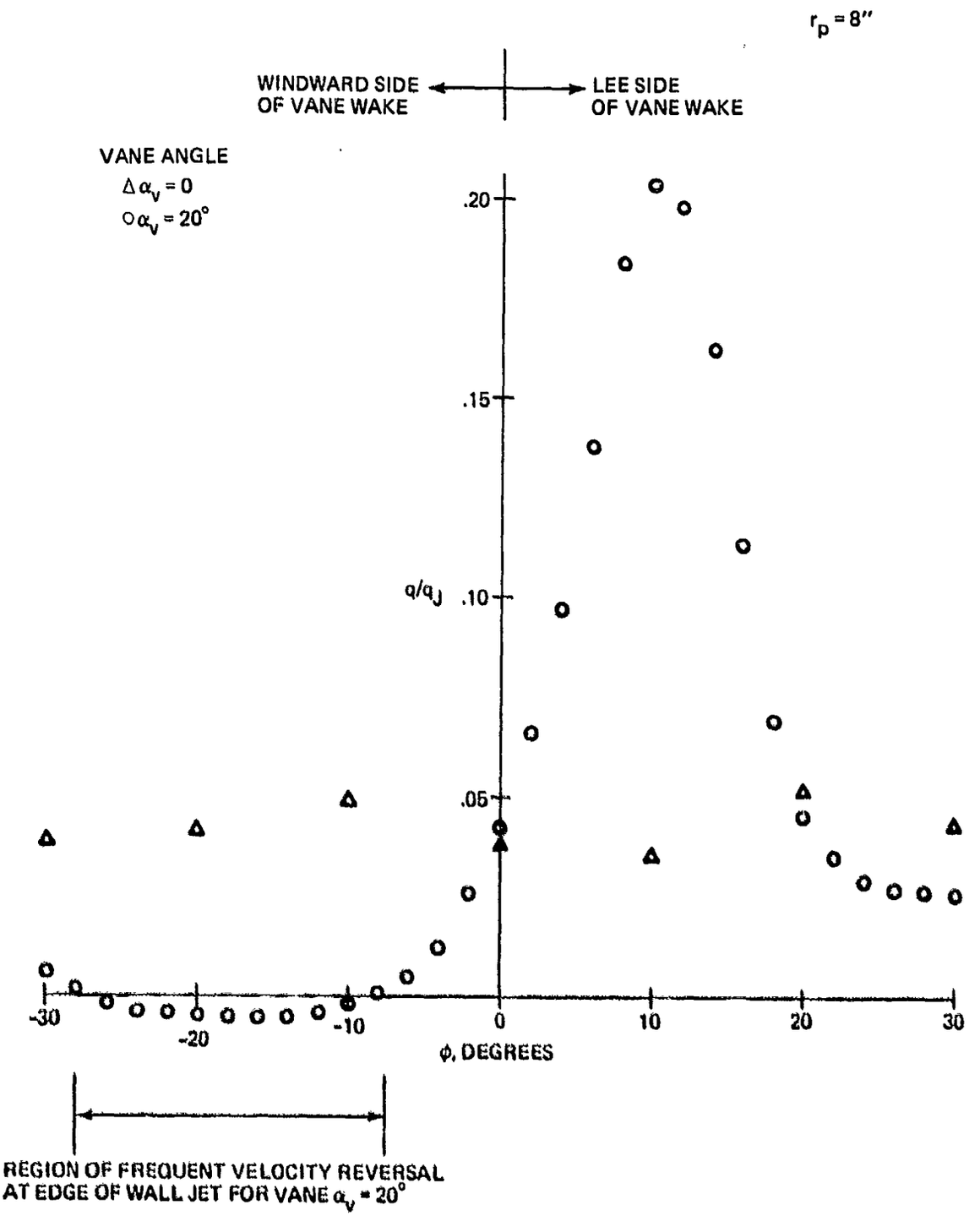

Figure 16 Wall Jet Strength at h' = 0.7 In.

We conclude that the presence of the vane at $\alpha_v = 0$ produces only minor changes in the impact region, based on small changes in the surface pressure distribution and oil flow patterns. Wall jet profiles show the same minor variations in thickness with azimuthal angle that existed without the vane. At a 20 degree vane angle of attack, severe distortions appear in the surface pressure distribution and in the streamline pattern. In the wall jet region there is a reduction in wall jet momentum parallel to the vane span-wise direction except for two locally concentrated regions of extremely thickened ground flow. These two thicker sections were symmetrically inclined 10° from the span direction for $\alpha_v = 20°$. The angle of inclination of these ground flow disturbances probably depends on α_v and perhaps also on h/d_f. In addition, the maximun wall jet velocity is increased in the direction $\phi = -90°$ (direction of incident flow deflection), and decreased in the opposite direction.

3. WALL JET PROPERTIES PRODUCED BY IMPINGEMENT OF A FAN JET ENGINE EXHAUST

The fan jet engine used in these tests consisted of a Lycoming T-55-L-11A turbojet that was coupled with a 4.6 foot diameter, 13 blade controllable pitch fan. This assembly was developed by Hamilton Standard as a prototype configuration for test purposes, and is known as the Q-Fan. The wall jet measurements described below were taken while the engine was on load to Grumman to evaluate the use of jet-immersed control surfaces for V/STOL applications. For this work the engine was mounted on a thrust stand with the exhaust directed toward a 20 foot square ground plane. Reference 6 presents a complete report on engine performance characteristics, control vane forces, vane surface pressures and temperatures, and the effects of varying ground plane location and orientation. In this report we present only those wall jet measurements that were taken with the ground plane normal to the exhaust, and with the ground plane located 40 inches from the van trailing edge unless otherwise noted.

Figure 17 shows a photograph of the ground plane. The large chute on the bottom was used to divert the wall jet behind the ground plane to avoid a possible interaction between the ground-deflected exhaust and the fan jet engine inlet. Two pitot pressure rakes, shown on the left edge of the ground plane, were used to measure wall jet conditions at two different radial locations. The inner rake was located 10 feet from the exhaust impact centerline and the outer rake was 12-1/2 feet from the centerline, with an azimuthal displacement of 37° relative to the inner rake.

Pressure signals from the two rakes (total of 18 pitot tubes) were read sequentially with a Scanivalve system, time-averaged, and displayed on a pen recorder. For each test condition (combination of ground plane location, vane location and engine operating condition) the control vane was driven through an angle of attack range. Pressure data were taken at each vane angle of attack. Since angle of attack settings were maintained for only 1 minute, there were only a few seconds available to record each pitot tube pressure. Signal fluctuations caused by variations in fan jet engine operating conditions could not be

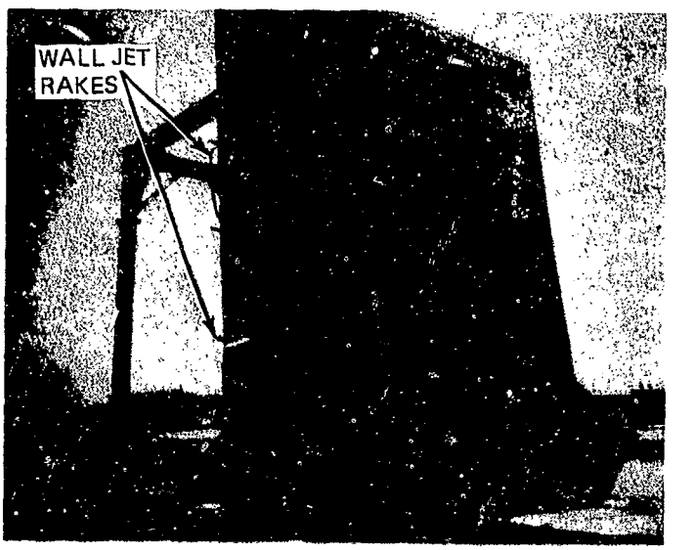

Figure 17 Ground Plane Used for Fan Jet Engine Impingement

sufficiently averaged on this time scale and provided a noticeable scatter in our measurements. On a typical run the measured engine thrust varied from 5800 to 6300 lb on a time scale of a few seconds.

Wall jet measurements obtained with zero vane deflection showed the same velocity profile shapes that we found in the model experiments. Figure 18 shows data taken from the inner and outer rakes with the ground plane normal to the flow at $h/d_f = 2$. Pitot pressures from each rake were normalized by the maximum pressure from that rake and the local velocities were plotted in the nondimensional form u/u_m. The probe location above ground was normalized by the half-velocity height $h'_{.5}$ for that rake. The solid line shown in Fig. 18 represents data that are shown in Fig. 6 for the wall jet formed by impingement of the simulated fan jet exhaust.

Measurements taken at the two rake locations provided a means of finding the radial decay in wall jet maximum velocity and the thickness growth rate for comparison with the smaller scale flows. Figure 19a shows the wall jet maximum velocity, normalized by the fan exit velocity, plotted against distance from the impact center in fan diameters. The solid line represents data shown in Fig. 8 that were obtained with similar impingement conditions using the simulated fan jet flow. Figure 19b shows a similar comparison for the radial increase in half-velocity thickness.

Deflection of the control vane changed the maximum velocity and the thickness of the wall jet. Figure 20a shows the variation of maximum wall jet velocity at the inner rake versus vane deflection angle for two different ground separation distances. The data show approximate symmetry around $\alpha_v = 0$ because of the inner rake location relative to the vane. Note that the maximum wall jet velocity at the inner rake does not decay significantly until vane angles exceed ±20°. Figure 20b shows that the maximum velocity at the outer rake is found for $\alpha_v = +10°$. For positive values of α_v the vane deflected the incident flow toward the outer rake.

Figure 21 shows pitot pressure profiles obtained from the inner rake at different vane deflection angles for normal ground plane impingement at $h/d_f = 2$. Note the strong increase in wall jet thickness that occurs even for small vane deflection angles. Data obtained from the outer probe did not exhibit any significant increase in wall jet thickness with vane deflection angle. This difference in wall jet behavior with vane deflection can be attributed to the different azimuthal orientation of the two probe rakes.

Figure 22 shows the variation of wall jet properties with azimuthal orientation. Three azimuthal orientations are shown (although only two rake locations were used) by assuming symmetry in the impingement flow. Since data were taken at $\alpha_v = +10°$ and $-10°$ at $\phi = 37°$, such data can also be viewed as for $\alpha_v = +10°$ with $\phi = +37°$ and $-37°$. To account for different radial locations of the measurements, the ordinate of the maximum velocity plot was scaled by the ratio $(\frac{r_p}{d_f})^{1.2}$. The exponent 1.2

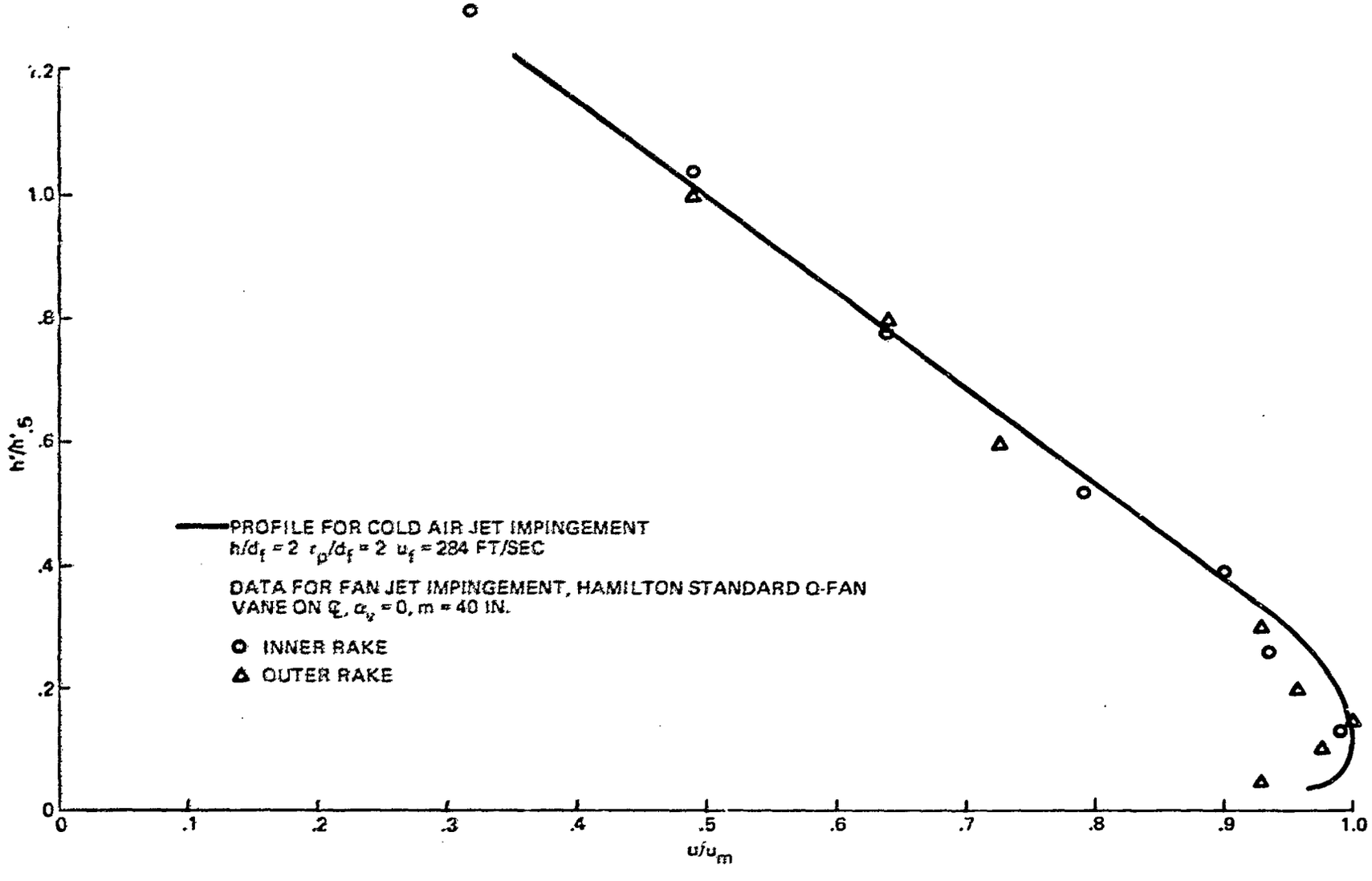

Figure 18 Comparison of Wall Jet Data From Engine Tests With Profile Obtained From Laboratory Simulation

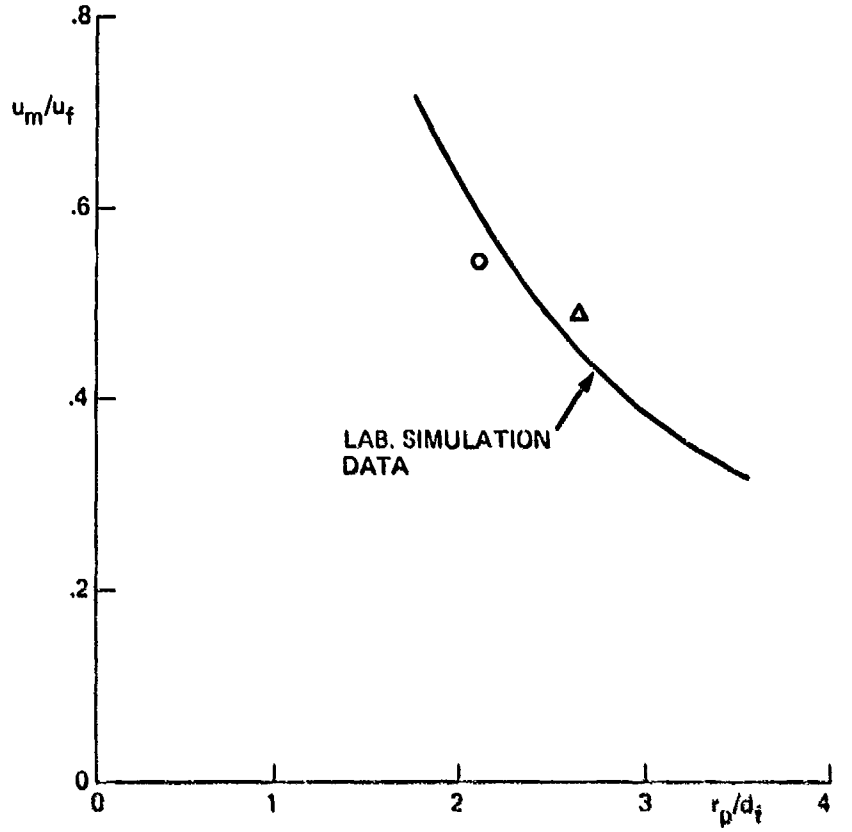

a) MAXIMUM VELOCITY DECAY
O INNER RAKE
Δ OUTER RAKE

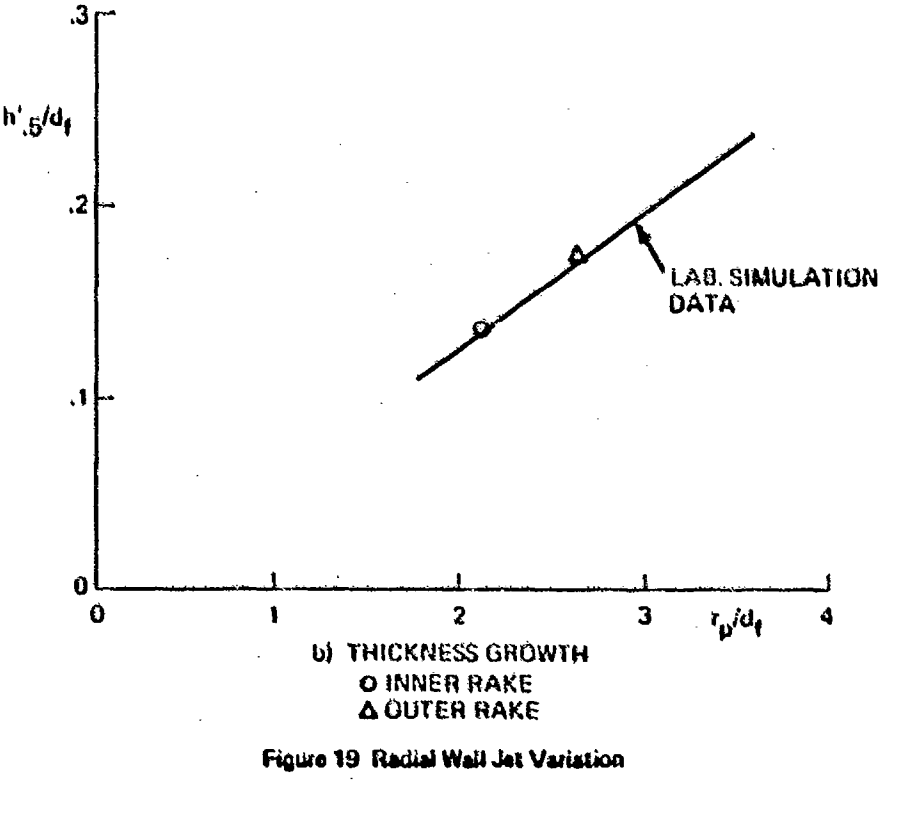

b) THICKNESS GROWTH
O INNER RAKE
Δ OUTER RAKE

Figure 19 Radial Wall Jet Variation

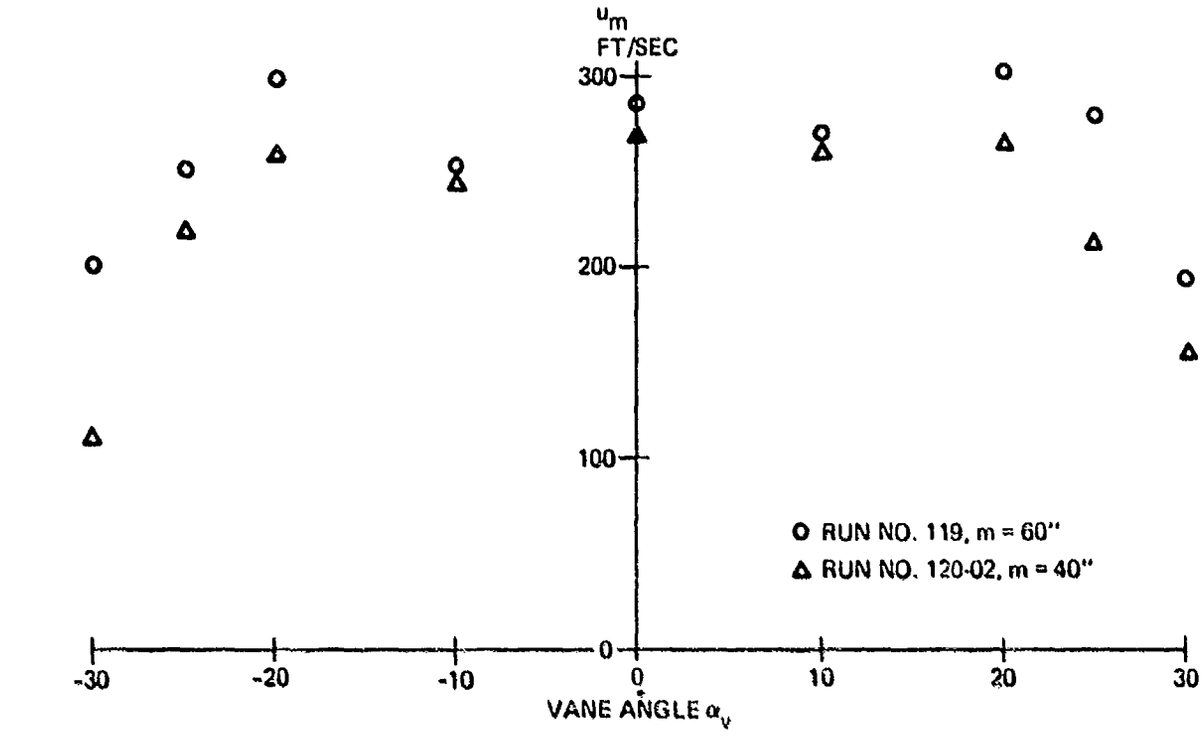

a) INNER RAKE

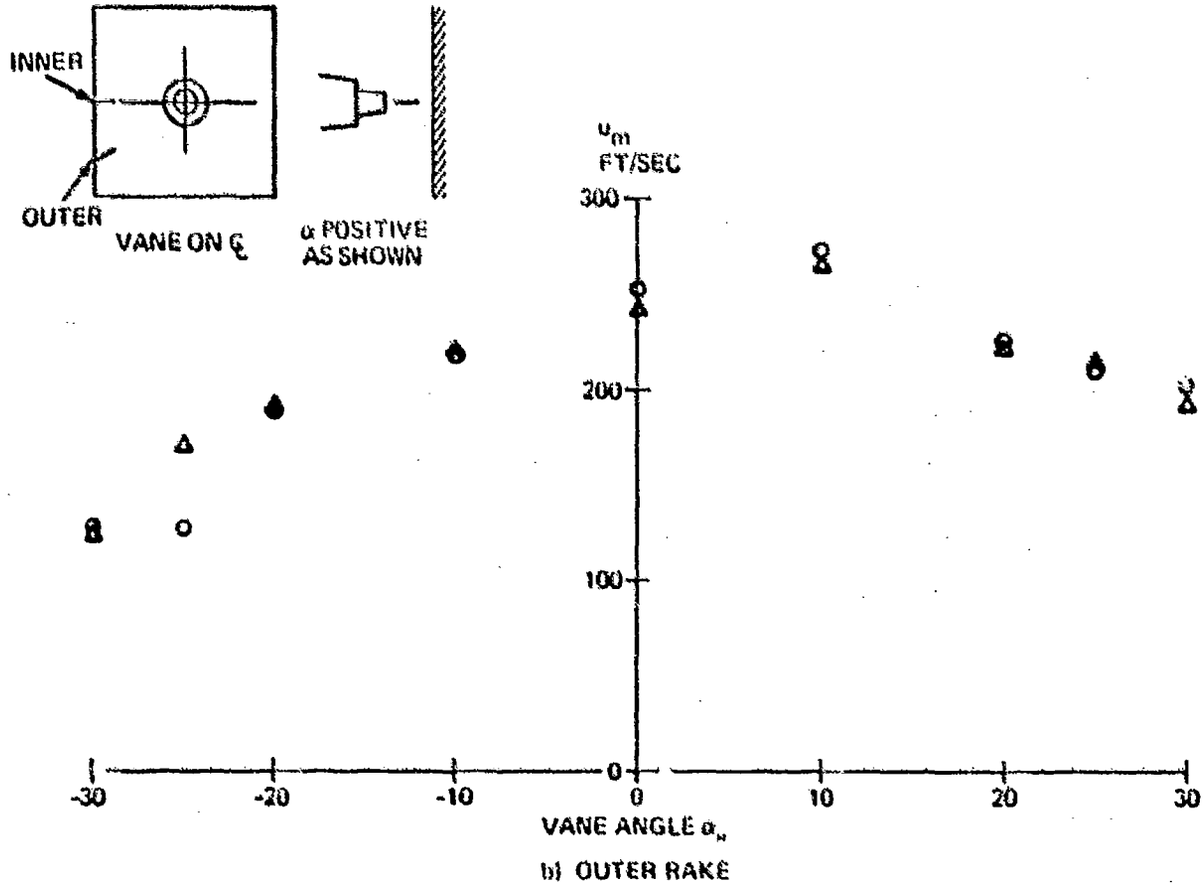

b) OUTER RAKE

Figure 20 Effect of Vane Angle on Maximum Wall Jet Velocities

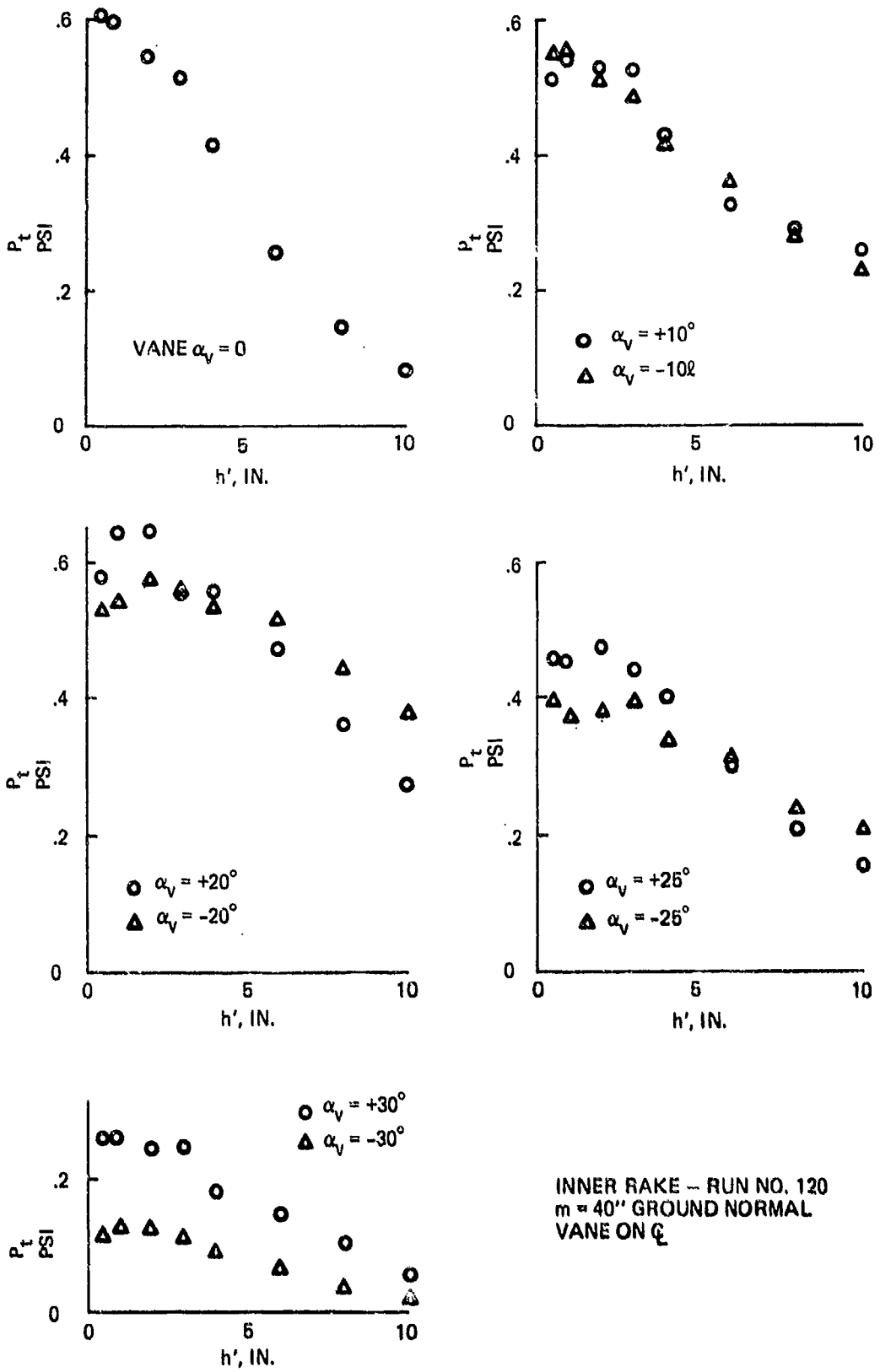

Figure 21 Wall Jet Profiles

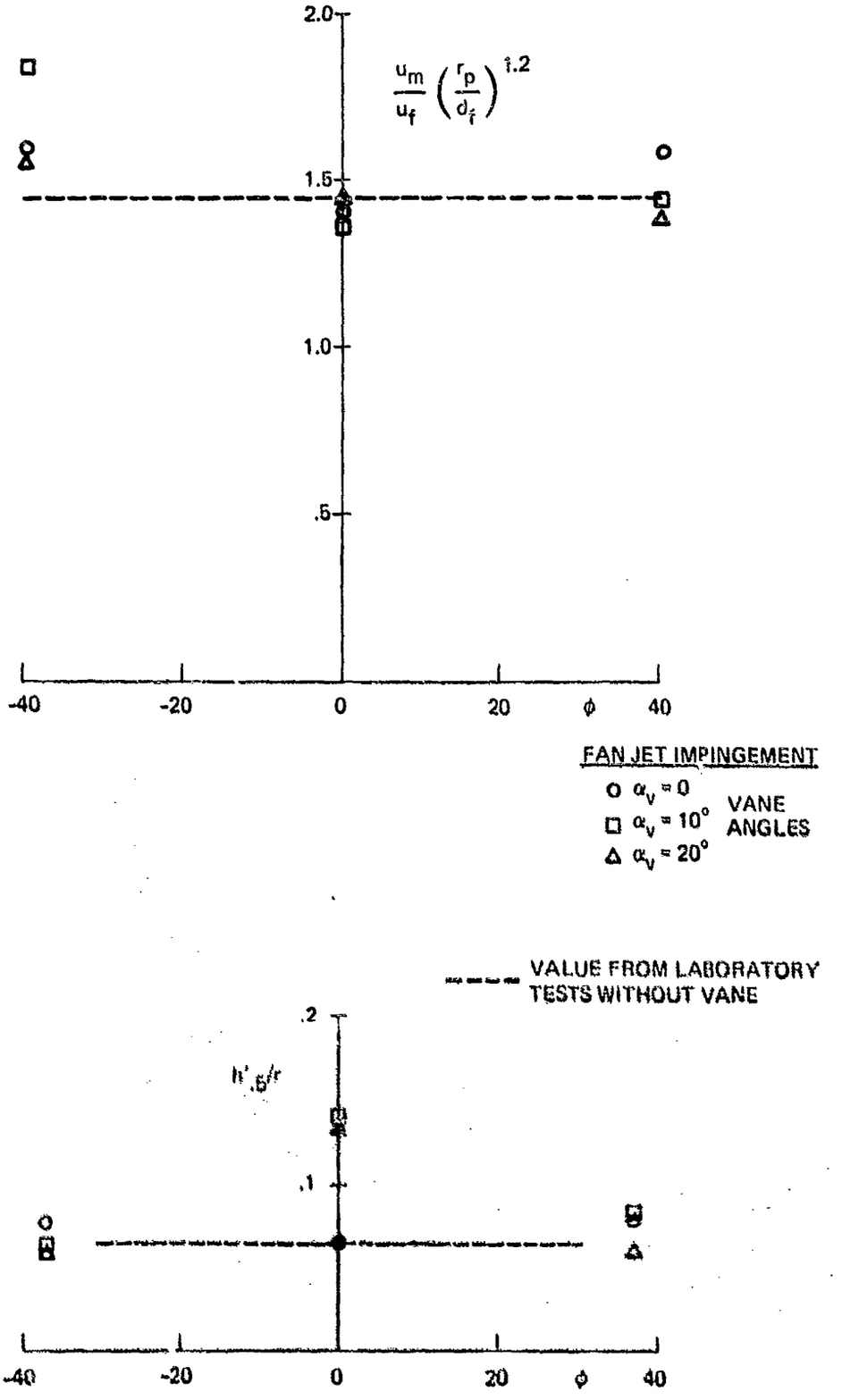

Figure 22 Effects of Vane Deflection on Wall Jet Properties

was found to account for the radial decay of wall jet maximum velocity in our laboratory tests without the vane. Vane deflection causes a thickening of the wall jet in the vane spanwise direction with no significant change in maximum velocity.

4. CONCLUSIONS

Normal impingement of a fan jet engine exhaust produces a ground flow pattern that is not axially symmetric. Ground surface pressure distributions show a local minimum near the center, with higher pressures around the periphery. The region of flow having lower dynamic pressure in the core of the incident jet escapes from the center of the impact zone through locally thickened regions of the ground flow. Factors affecting the locations of the thickened ground flow could not be identified, but these locations were sensitive to ground plane alignment and nozzle geometry. These local disturbances in the impact region extended outward radially to produce a nonsymmetric distribution of wall jet properties.

Velocity profiles in the wall jet region beyond two fan diameters from the impact center exhibited the same shape as those obtained in a wall jet formed by normal impingement of a simple round jet. This agreement in velocity profile shape was found at all azimuthal locations in spite of local variation in wall jet thickness and maximum velocity. However, the radial velocity decay and thickness growth rate agreed with simple round jet impingement data only at azimuthal locations that did not exhibit local thickening.

The presence of a control vane in the fan jet exhaust at zero angle of attack produced only a minor change in the impingement pattern. Inclination of the vane locally concentrated the wall jet flow to produce a small area of thickened ground flow located near the axis of the vane. In addition, the maximum wall jet velocity generally increased in the windward side (direction the jet flow was deflected) and decreased on the lee side.

Scale effects on wall jet behavior were evaluated by comparing wall jet data taken during ground impingement of a real fan jet engine exhaust with measurements obtained in a small scale simulation of this flow. For zero vane deflection the wall jet profiles in both flows exhibited the same shape. The radial decay in maximum velocity and thickness growth agreed well when scaled by fan exit velocity and diameter, respectively.

5. REFERENCES

1. Jenkins, R.C. and Hill, W.G., Jr., "Investigation of VTOL Upwash Flows Formed by Two Impinging Jets," Grumman Research Department Report RE-548, November 1977.

2. Glauert, M.B., "The Wall Jet," J. of Fluid Mech., Vol. 1, December 1956, pp. 625-643.

3. Donaldson, C. DuP. and Snedeker, R.S., "A Study of Free Jet Impingement - Part I - Mean Properties of Free and Impinging Jets," J. of Fluid Mech., Vol. 45, Part 2, pp. 281-319, 1971.

4. Siclari, M.J., Hill, W.G., Jr., and Jenkins, R.C., "Investigation of Stagnation LIne and Upwash Formation," AIAA Paper No. 77-615, AIAA/NASA, Ames V/STOL Conference, June 1977.

5. Hill, W.G., Jr., and Jenkins, R.C., "Experimental Investigation of Multiple Jet Impingement Flows Applicable to VTOL Aircraft in Ground Effect," Grumman Research Department Memorandum RM-605, November 1975.

6. Rice, R., et. al., "Large Scale Static Test of an Integrated V/STOL Propulsion/Attitude Control System," Grumman Advanced Aircraft Systems Report, to be published.

7. Gauntner, J.W., Livingood, J.N.B., and Hrycak, P., "Survey of Literature on Flow Characteristics of a Single Turbulent Jet Impinging on a Flat Plate," NASA TN D-5652, February 1970.

APPENDIX

CHARACTERISTICS OF WALL JETS FORMED BY CIRCULAR JET IMPINGEMENT

Impingement of a free jet on a flat ground plane produces a radial flow along the ground as shown in Fig. A-1. The impact region is characterized by high surface pressure and extreme local flow curvature. In the transition zone the flow completes turning parallel to the ground. The relative sizes of these two inner regions depend on the ground separation distance h/d. In the wall jet region the velocity profile is controlled by turbulent mixing and entrainment of ambient air except for a region close to the ground that shows a boundary layer profile.

Velocity profiles taken at different radial stations in the wall jet region show similar shapes when nondimensionalized by maximum velocity and by half-velocity thickness. Figure A-2 shows such profiles taken at two radial stations in the wall jet formed by impingement of a four-inch diameter jet. The data obtained for two different jet exit velocities at r/d = 1.75 illustrates the profile shape near the end of the transition zone where the actual wall jet profile is not fully formed. The shape shown by the triangles was found for radial locations greater than r/d = 2 with minor variations caused by boundary layer growth. The velocity profiles at different radial stations in the wall jet region cannot be exactly similar because the boundary layer thickness grows at a different rate than the wall jet thickness.

For a wall jet formed by normal impingement of a circular jet, Donaldson and Snedeker (Ref. 3) have modeled the wall jet radial characteristics with a decay in maximum velocity u_m that is proportional to $r^{-1.1}$ and an increase in half-velocity thickness that is proportional to $r^{1.01}$. They found these values to be valid at least over the Reynolds number range from 10^4 to 2×10^5 based on wall jet thickness. Because the wall jet profiles exhibit similarity, this model can be used to describe the radial decay of either the maximum velocity or the average velocity of the wall jet.

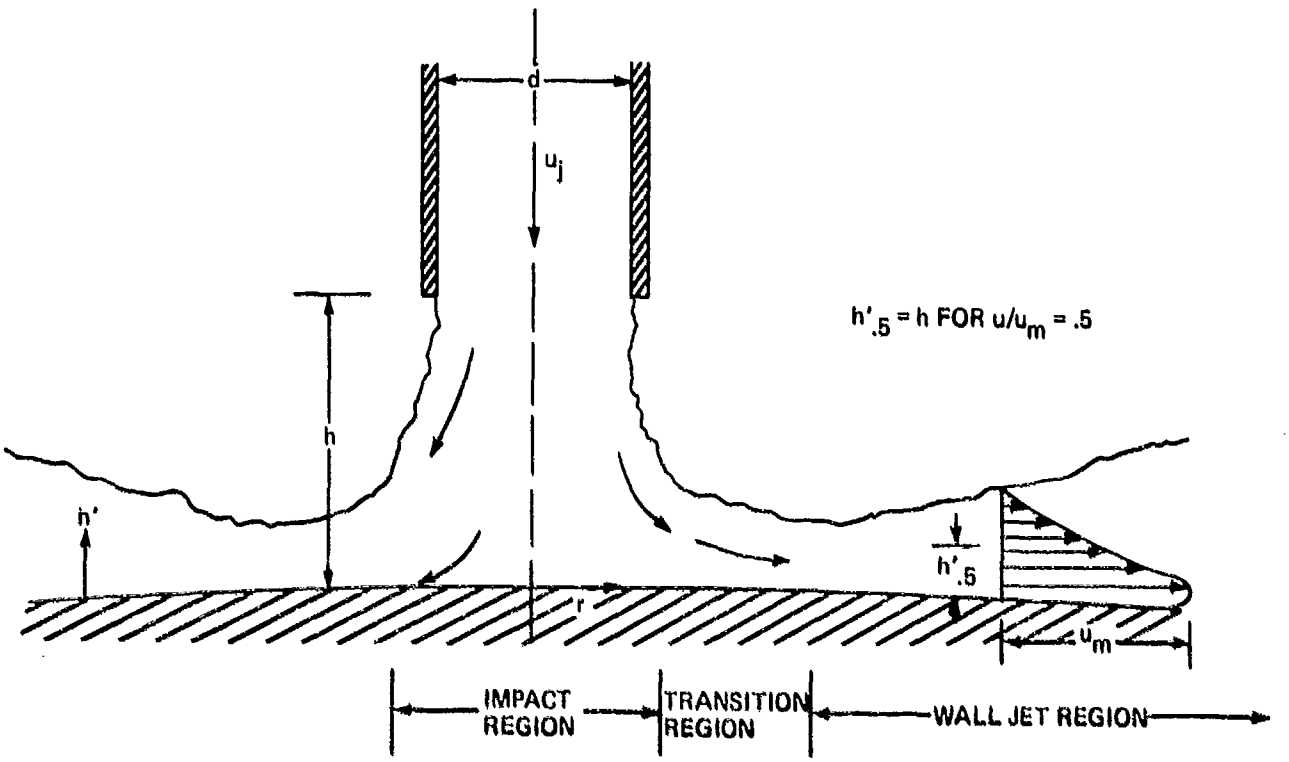

Figure A-1 Sketch of Free Jet Ground Impingement

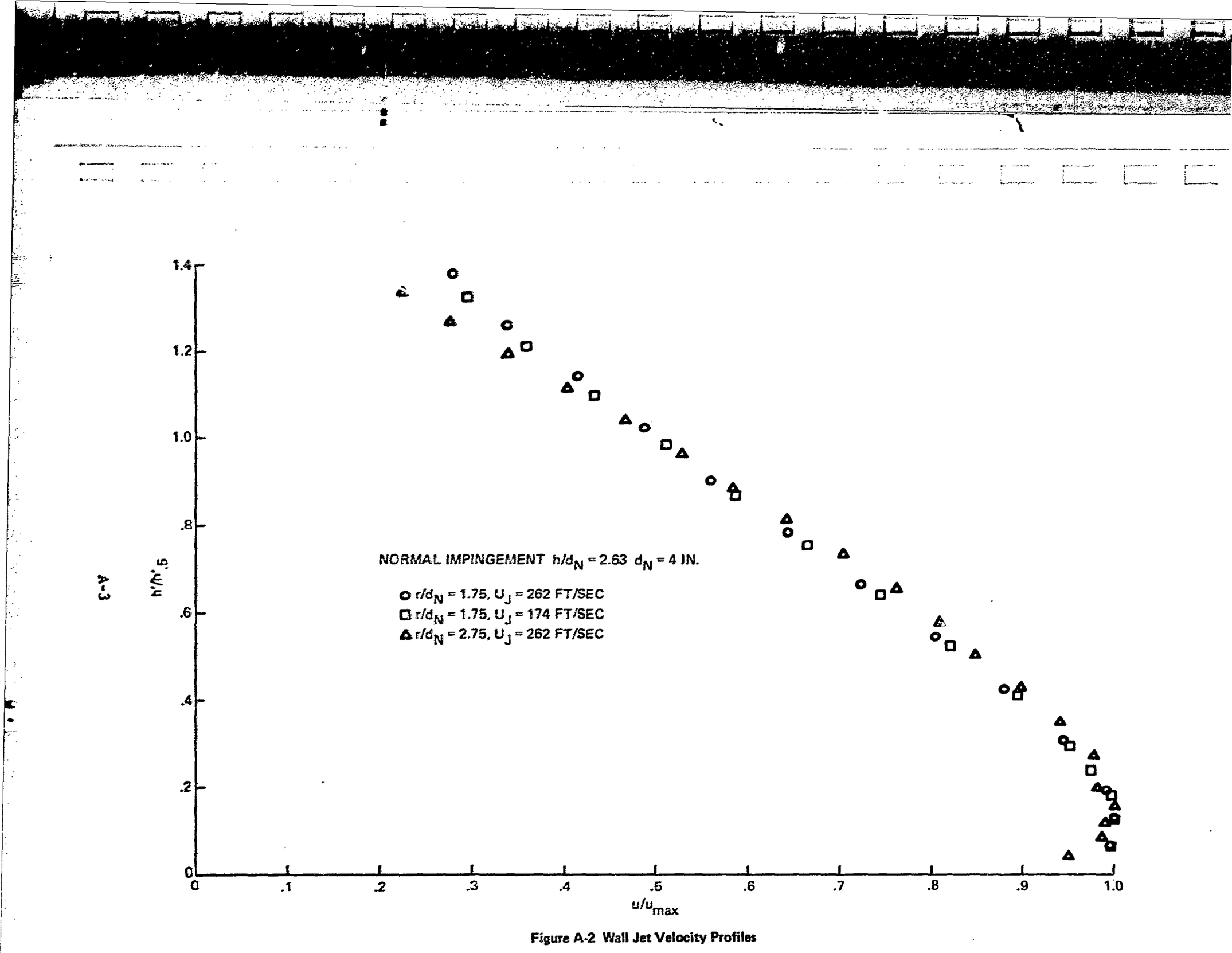

Figure A-2 Wall Jet Velocity Profiles

Similarity of wall jet profiles allows the flow at a given point on the ground to be described by the local values of maximum velocity u_m and half-velocity thickness $h'_{.5}$. Figure A-3 shows the variation of wall jet properties with ground plane spacing for a four-inch diameter round jet. Maximum velocity was normalized by jet exit velocity and half-velocity thickness by the probe distance from the impingement center. These data were all taken with the probe located four diameters from the center. The wall jet properties show little variation with ground plane spacing except for $h/d \leq 3$.

Figure A-4 shows the radial decay in maximum velocity of a wall jet formed by normal impingement of a four-inch diameter jet for three nozzle exit velocities. The data show no effect of incident jet velocity on the slope and a negligible effect on u_m/u_J values. The radial decay in maximum wall jet velocity found from these data is given by $u_m \sim r^{-1.24}$.

Figure A-5 shows the half-velocity thickness of the wall jet at different radial locations for the same three incident jet velocities. The effect of jet velocity had only a minor influence on the slope. A line drawn through the data, extropolated back through the impingement zone, does not pass through the impingement centerline. This point has been noted by other investigators, who have attempted to represent the half-velocity growth by the power law variation

$$h'_{.5} \sim r^n$$

where n is close to 1. A value of 1.04 would fit our data, which can be compared to the value n = 1.01 given in Ref. 3.

Since our data were obtained at Reynolds numbers between 10^4 and 1.5×10^4, differences between our results and the model proposed by Donaldson and Snedeker should not be attributed to Reynolds number alone. Other investigators (data reviewed in Ref. 7) found that slightly different exponents of r provided a better fit to their data. The reason for these differences, which is still under active investigation, may be caused by the nozzle size or by the separation distance between nozzle and ground.

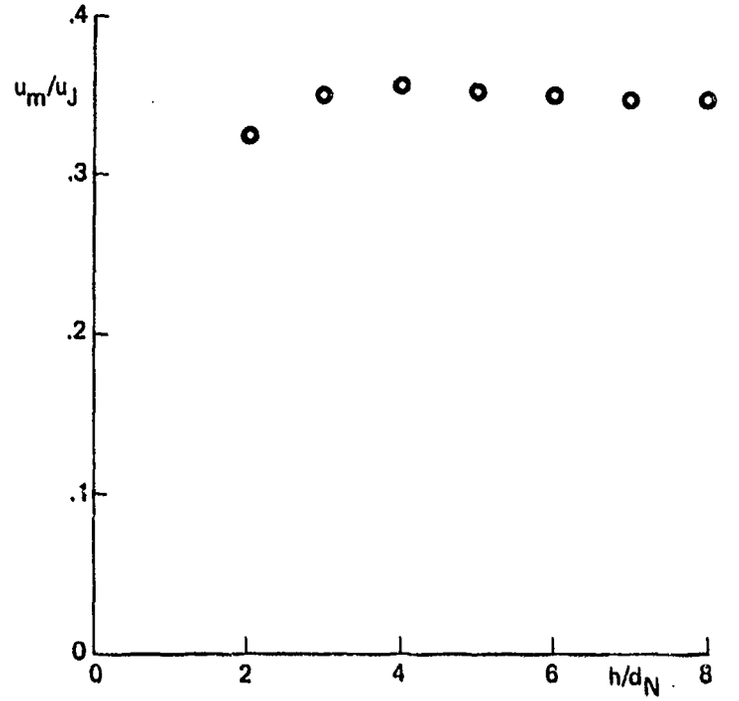

a) MAXIMUM VELOCITY AT $r_p/d_N = 4$

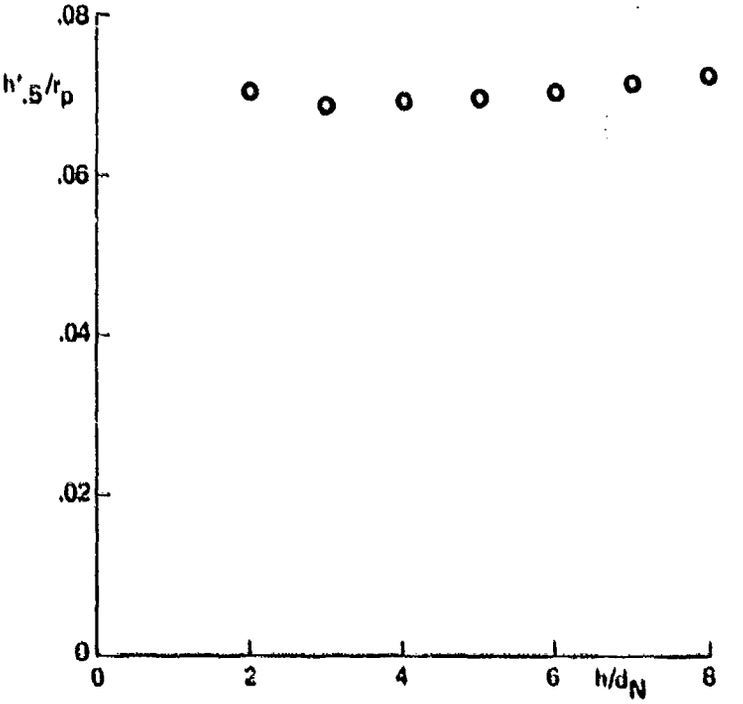

b) THICKNESS AT $r_p/d_N = 4$

Figure A-3 Effect of Ground Spacing on Wall Jet Characteristics

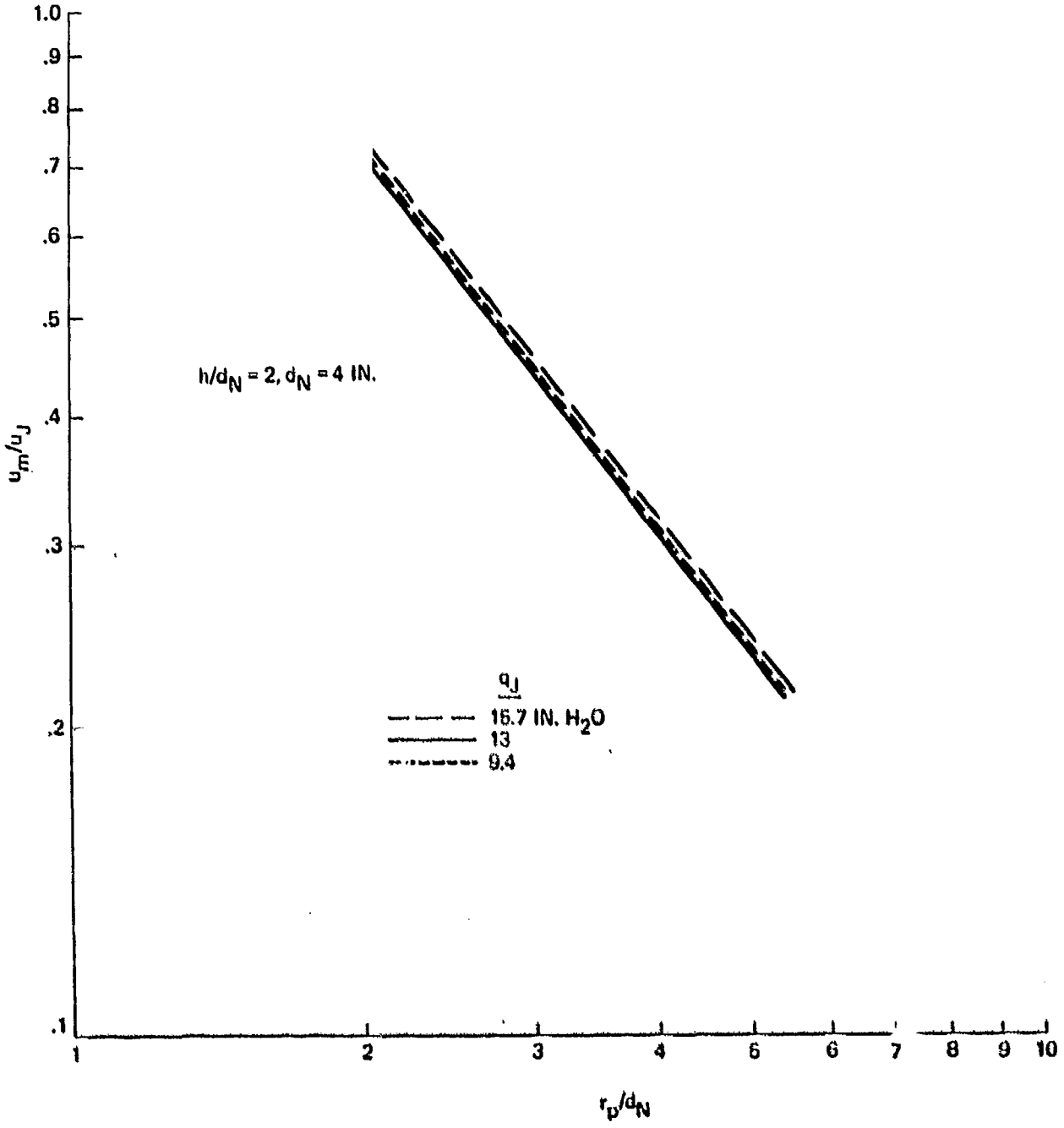

Figure A-4 Effect of Jet Velocity on Radial Decay of Maximum Wall Jet Velocity

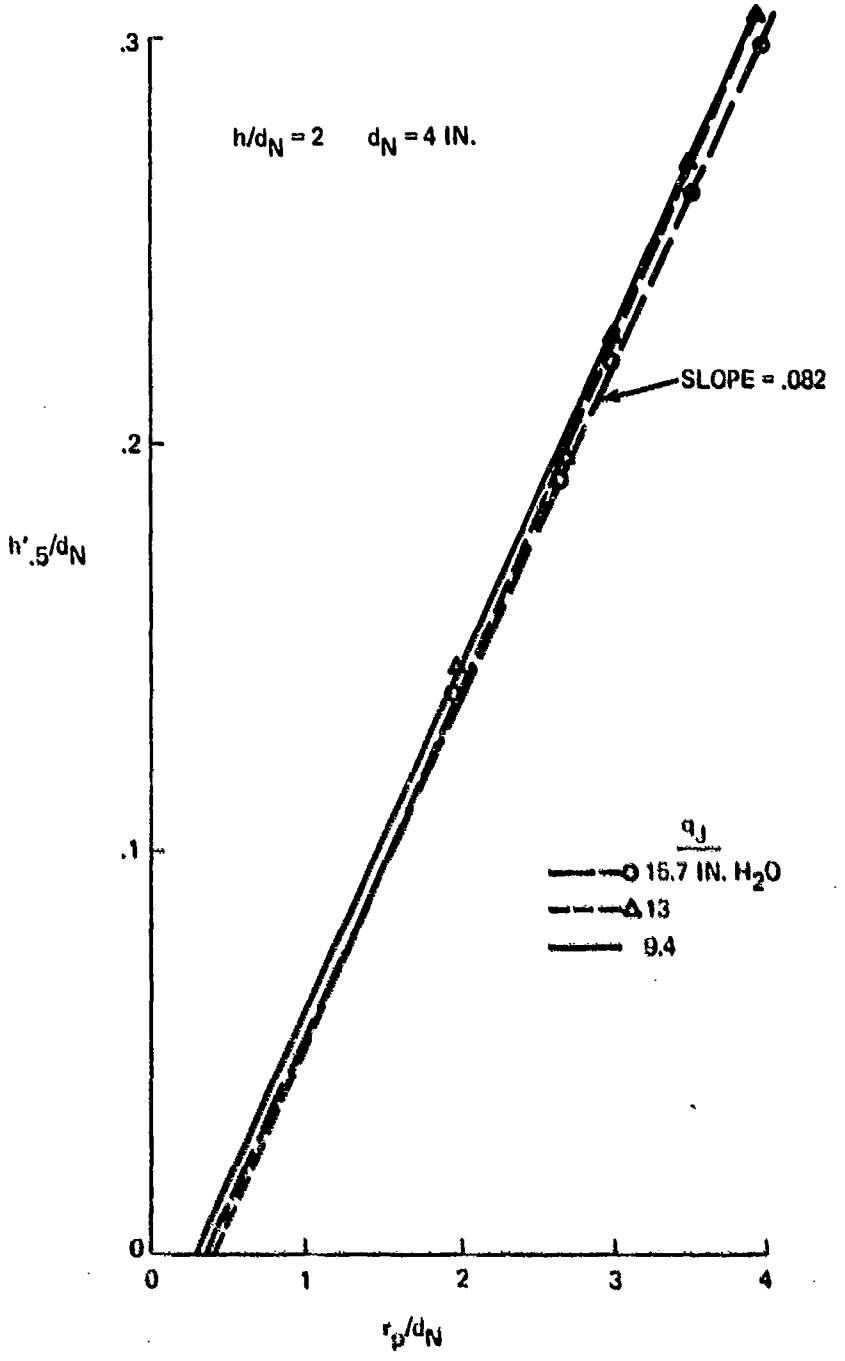

Figure A-5 Effect of Jet Velocity on Wall Jet Growth